SUBMISSION TO
INTERNATIONAL JOURNAL OF GEOMECHANICS

DATE: 27/01/2021
Written: November 2021
Revised: May 2022

TITLE:
Climate change adaptation of Elbe River flood embankments via suction-based design

AUTHORS:
Raniero Beber[1]
Alessandro Tarantino[2]
Patrick Becker[3]

AFFILIATION:
[1] Department of Civil and Environmental Engineering, University of Strathclyde, 75 Montrose Street, G11XJ, Glasgow, UK (raniero.beber@strath.ac.uk)

[2] Department of Civil and Environmental Engineering, University of Strathclyde, 75 Montrose Street, G11XJ, Glasgow, UK (alessandro.tarantino@strath.ac.uk)

[3] Kempfert Geotechnik GmbH, Hasenhöhe 128, 22587 Hamburg, Germany (p.becker@kup-geotechnik.de)

CORRESPONDING AUTHOR:
Raniero Beber
Department of Civil and Environmental Engineering
University of Strathclyde
James Weir Building - Level 5
75 Montrose Street - Glasgow G1 1XJ, Scotland, UK
E-mail: raniero.beber@strath.ac.uk

KEYWORDS
Flood embankment, performance-based design, land expropriation, habitat suppression, embodied carbon

Climate change adaptation of Elbe River flood embankments via suction-based design

Abstract

Flood embankments are generally designed by assuming steady-state flow conditions and dry soil above the phreatic surface. However, steady-state conditions are rarely achieved and a significant portion of the embankment remains unsaturated upon a flood event. If transient water flow and partial saturation are considered, the flood embankment can be designed with steeper slopes on the landside, which may lead to significant savings in terms of earthfill material (i.e. embodied carbon) and footprint (i.e. habitat suppression and expropriation costs). This paper examines the case of flood embankments in the tidal area of the Elbe River in Germany. These embankments require to be retrofitted by raising their crest from 5m to 7m because of the new projection of extreme river levels due to climate change. In this paper, the conventional 'prescriptive' design consisting of raising the embankment by maintaining the 1:3 inclination of the landside slope is compared with the 'performance-based' design where the inclination of the slope on the landside could be potentially increased up to 1:1, which is shown to be sustainable if partial saturation and transient water flow are considered. Raising the flood embankment with 1:1 landside slope (rather than 1:3) could lead to expropriation cost savings of the order of €3.9M/km. For the case of a newly built embankment of 7 m height, the saving would become €4.5M/km. An approximate estimation of embodied carbon suggests that the carbon saving would be of the order of 3,100-4,200tCO2e/km.

Introduction

The increase of extreme weather events is a well-established trend observed as a consequence of climate change. In the North Sea, storm surges are anticipated to increase in both intensity and duration (Barnard et al. 2019) and there is therefore a need to protect communities from the increased flood hazard.

Earthen structures such as flood embankments are the main asset to manage and mitigate flood risk. Increased extreme sea levels require upgrading flood embankments by raising their crest. Retrofitting measures should be designed to maximise social (reduced flood risk hazard) and economic (lowering costs of flood protection maintenance) benefits and minimise environmental impact due to habitat suppression and carbon emissions (Defra 2002; Spencer and Harvey 2012; Committee on Climate Change 2013; Spalding et al. 2014).

If the flood embankments are raised with the same prescribed inclination of the landside slope (e.g. 1:3 in the Elbe River area in Germany), the footprint of the upgraded flood embankment would increase significantly posing two major problems. Existing earthen structures are often adjacent to the built environment and there is either no space available to increase the embankment footprint or this is associated with high land expropriation costs. At the same time, environmental legislation such as the European Birds and Habitats Directives (Sundseth, 2012) imposes constraints to prevent the loss and degradation of coastal habitats and associated biota. The increase in flood embankment footprint associated with the increase of its crest generates direct and indirect loss of habitat, which requires to be compensated elsewhere. The lesser the generation of footprint by the retrofitted flood embankment, the lower are the direct and indirect economic and environmental costs.

This calls for new approaches to embankment design, i.e. raising crest level by limiting the increase in embankment footprint. This would also limit flood embankment embodied carbon.

Construction is one of the main sectors responsible for carbon emissions and geotechnical engineers are challenged to develop new design concepts for carbon-efficient geo-infrastructures. Suction and partial saturation are commonly neglected in geotechnical design. However, suction is an extraordinary untapped natural 'reinforcement' and could significantly contribute to reduce economic and carbon costs of a geostructure if accounted for in geotechnical design.

In this respect, it is worth highlighting that design of river, estuarine, and coastal flood embankments based on transient water flow is now being introduced in national recommendations including Germany (Committee for coastal protection works of the German Society for Earthworks and Foundation Engineering and the Society for Port Engineering, 2020). This implicitly acknowledges the economic and environmental benefit of suction-based design. The importance of partial saturation and transient-state conditions for a realistic assessment of the existing safety conditions of flood embankments is also highlighted by Gragnano et al. (2021) who monitored a river embankment on the river Secchia (northern Italy) for 36 months. The importance of partial saturation in the analysis of the response of flood embankments is now widely acknowledged in the literature (Vahedifard et al. 2022; Ngo et al. 2022; Zhang et al. 2021; Johari et al. 2019; Khalilzad et al. 2015).

A critical aspect in suction-based design is that loss of suction due to rain-water and/or river-water infiltration. However, Showkat et. al. (2022) showed that, if properly modelled, the suction-based design of earthen structures is feasible for practitioners that nowadays commonly use more advanced computational models. Another critical aspect of suction-based design is the reliable characterisation of the unsaturated soil hydraulic behaviour. For example, Bhaskar et al. (2022) observed that the saturated hydraulic conductivity was found to be 15 times lower after the soil experienced a drying and wetting cycle. This highlights the importance of considering the effect of hysteresis on hydraulic.

This paper aims at examining whether, and to what extent, the inclusion of soil suction and partial saturation in geotechnical design of flood embankments (including the analysis of water flow under transient conditions instead of the conventional steady-state approach) could reduce the flood embankment footprint and embodied carbon while keeping the performance of the flood embankment to the required geotechnical standard. The analysis is developed herein with reference to the design of the upgrade of Elbe River flood embankments in the Hamburg tidal area in Germany. However, similar concepts could be applied to the retrofitting of existing infrastructures that has to be raised in order to meet new design water levels in other countries.

The Hamburg flood defence system

Historical floods and upgrade of flood protection infrastructure

Hamburg is located on the Elbe River in northern Germany with 270 km^2 of its metropolitan area considered at risk of flooding (including 180k inhabitants and €10 billion worth of goods). The flood defence system extends over 260 km and consists of 130 km of earthen embankments. It is designed to prevent overflow of the Elbe River mainly associated with the storm surges in the North Sea.

The two most catastrophic storm surge events in the 20th century occurred on 16-17 February 1962 and 3 January 1976. The first event was characterised by a water level mark of +5.7 m above NN (NN stands for Normal-Null, i.e. standard elevation zero adopted in Germany until 2000) and 80mm of rainfall in 24 h, which flooded 30% of the city and caused 315 fatalities. The second event devastated the harbour area with a water level mark of +6.45 m above NN (von Storch 2017).

Since the 1976 event, the flood protection infrastructure has been upgraded repeatedly including a major investment of €660M in the period 1998-2015. The Hamburg city council has recently launched a programme to further raise flood defence embankments from 5.7 to 7m above landside ground level (7.7 to 9m above NN) to accommodate the increase extreme sea levels due to global warming (Vousdoukas et al., 2018).

Embankment typical cross section and geological setting

The typical cross section of the flood embankments in the Hamburg area consists of 1:3 slopes with a crest 3 m wide. The embankment core is generally constructed with locally sourced sand whereas the outer shell consists of an impermeable cover (clayey silt named 'Klei') with thickness greater than 1.3m and 1.0m on the waterside and landside respectively. The slope becomes gentler at the toe on the river side (1:10 or 1:6) often armoured with stones to prevent erosion of the bank due to tidal fluctuations and waves.

The Hamburg flood embankments are built on a Holocene sedimentary deposit. The upper soil layers are made of silty sand (qe-Elster glaciation) and/or klei (qh-Holocene) as shown in Figure 1. Three scenarios were considered to represent typical soil profiles under the flood embankments as illustrated in Figure 3, i) uniform silty sand layer (L0), ii) klei and peat layer overlying a layer of silty sand (L1), and iii) a sandwich of silty sand, klei and silty sand layers (L2).

Design storm surge

The Hamburg Port Authority (HPA) has developed a technical framework to design adaptation measures for private flood protection in the Hamburg tidal region (HPA 2008). This includes the adoption of standard design storm surges as shown in Figure 2. These two storm surges represent two different scenarios, that is relatively long duration of surge (~50h) with moderate peak surge elevation (6 m above NN) and relatively short duration of surge (~30h) with high peak surge elevation (7.3 m above NN). These two scenarios will be used as a basis for the analyses presented in this paper.

Methodology

The standard design of flood embankments based on steady state water flow and assuming zero-pore water pressures above the phreatic surface was compared to the design based on transient water flow and assuming the soil to be unsaturated above the phreatic surface. To this end, numerical simulations were carried out to compare these two different design approaches. The soil was assumed to have a rigidly-perfectly plastic behaviour thus allowing uncoupling water flow analysis from slope stability analysis. The numerical analyses were intentionally kept simple to makes the analyse easily accessible to engineers.

Flood embankment cross section

The analyses were performed by considering the typical cross section with landside slope 1:3 and increasing progressively up to 1:1 (Figure 3). The aim was to explore whether and to what extent the embankment can be designed with steeper slopes if unsaturated soil and transient flow are considered.

Three different foundation scenarios (L0, L1, and L2) were considered as shown in Figure 3 to be representative borehole logs shown in Figure 1. The embankments and their foundations are formed by three materials, a clayey silt referred to as ‘klei’, a sand, and a silty sand.

Materials

The grain size distribution of materials forming the flood embankments and their foundations are shown in Figure 4 and were extracted from a database compiled the Hamburg Geological Survey (GLH, 2017).

Water retention and hydraulic conductivity characterisation

Standard geotechnical tests available for the Hamburg area have been carried out only on materials in the saturated state. A simple engineering approach was adopted to characterise the materials' water retention behaviour. The parameter that most characterises a water retention function is the air-entry suction because it varies by several orders of magnitude when moving from coarse-grained to fine grained materials. The air-entry suction is controlled by the larger pore-sizes in turn associated with the larger grain size as a first approximation. Tarantino and Di Donna (2019) have shown that the air-entry suction can be related to particle size corresponding to the 80% finer fraction, D80 (Figure 24 in Tarantino and Di Donna, 2019). Although such an empirical relationship was built on a relatively small dataset, its peculiarity is that it was developed by considering only undisturbed non-agricultural soils. The values of air-entry suction sAEV derived from this empirical correlation based on the grain size distributions curves in Figure 4 are presented in Table 1.

The 2-parameter van Genuchten soil water retention function shown in Eq. [1] (van Genuchten, 1980) was adopted to model water retention behaviour.

$$\theta_e = \frac{\theta}{\theta_s} = \left[\frac{1}{1+(\alpha s)^n}\right]^m \qquad \left[m = 1 - \frac{1}{n}\right] \qquad [1]$$

where θ is the volumetric water content, θ_{sat} is the volumetric water content at saturation, θ_e is the effective degree of saturation, and α and *n* are soil-dependent parameters. The parameter *n* was estimated using engineering judgement considering that *n* increases as the grain size uniformity coefficient decreases. Once *n* was fixed, the parameter α was determined to match the air-entry suction s_{AEV} estimated empirically (Table 1Table 1). The resulting water retention functions are shown in Figure 5.

The hydraulic conductivity *k* was characterised based on van Genuchten (1980):

$$k = k_{sat} \cdot \left\{\sqrt{\theta_e}\left[1 - \left(1 - {\theta_e}^{1/m}\right)^m\right]^2\right\} \qquad [2]$$

where k_{sat} is the saturated hydraulic conductivity derived from the database made available by the Hamburg Geological Survey (GLH, 2017) as shown in Table 1.

Shear strength characterisation

Shear strength parameters for the Sand and Silty Sand were derived from a table made available by the Hamburg Geological Survey (GLH, 2017) and are shown in **Table 2**. The values of the friction angle ϕ' and effective cohesion *c*' for these two materials are in the range expected for the grain size distributions shown in Figure 4. On the other hand, the values of ϕ' and c' for the klei were somehow contradictory. Significantly different values were reported for Consolidated Drained (CU) and Consolidated Undrained (CU) triaxial tests and a wide range of pairs of (ϕ', c') were provided (see Appendix 1). Two options were therefore considered. The data for the values of ϕ' and c' reported by the Hamburg Geological Survey (GLH, 2017) for drained tests where first correlated (as expected the friction angle ϕ' decreases as the effective cohesion c' increases) and the average values were selected as shown in **Table 2** as option 1 (see Appendix 1). The available raw triaxial data were then examined and values ϕ'=30° and c'=0 were selected as discussed Appendix 1 (shown in **Table 2** as option 2). The two options allow considering the cases of zero and non-zero effective cohesion.

Embankment crest and slopes are generally turfed, i.e. the uppermost layer of the embankment is reinforced by the root system. To take into account the mechanical effects of roots, to the uppermost klei layer of the embankment (200 mm) was assigned an effective cohesion of 4 kPa. This is in line with the values reported in the literature (De Baets, 2008; Comino, 2010, Baral et al., 2019).

Water-flow model

The Software GEOSTUDIO 2019 was used for the analyses. It includes the module SEEP/W to compute the pore-water pressure and the module SLOPE/W to perform the stability analysis using the simplified Bishop method of slices (GeoSlope 2019)

Governing equation

The governing equation (Lu and Likos 2004, Eq. S1 in Supplemental Materials) was solved numerically using the FEM code SEEP/W. It was assumed that the soil skeleton is rigid and, hence, the hydraulic flow is uncoupled from the mechanical deformation (i.e. the volumetric water content θ only depends on the pore water pressure u_w). A coupled hydro-mechanical model would have added unnecessary complexity considering that the water retention behaviour and the relative hydraulic conductivity thereof were estimated using informed engineering judgement.

Hydraulic initial and boundary conditions

The initial condition for the transient analysis was generated via a steady-state seepage analysis with hydraulic head on the river side set to 0 m NN. The hydraulic boundary conditions were assigned as follows (see also Figure S2 in Supplemental Materials):

1) Constant hydraulic head assigned to the vertical boundary on the landside to simulate far-field ground water table (0 m NN corresponding to 2m below the ground surface). The distance of the landside vertical boundary from the toe of the embankment was set to 52-67m depending on the embankment landside slope considered. The extension of the flow domain was wide enough to not affect the pore-water pressure distribution up to 10 m from the toe of the embankment.
2) Bottom boundary modelled as impermeable.
3) Crest of the embankment, landside slope and landside ground surface were modelled as potential seepage faces, i.e. water flux is imposed equal to zero as long as the pore-water pressures remains negative (u_w<0), otherwise pore-water pressure is set equal to zero (Figure S2).
4) Transient water flow - Boundary condition on the water side was designed as shown in Figure 6. The river water level was allowed to fluctuate for 1 year to simulate the normal tide regime with the water level oscillating between the lower tide water level (MLT=-1.90m NN) and the high tide water level (MHT=+2.42m NN). This was followed by the storm surge over a period of 100h. Two different patterns were considered for the storm surge as shown in Figure 6 according to the standard design storm surges developed by Hamburg

Port Authority (Figure 2) with water level peaks of 6m NN (A) and 7.3m NN (B) respectively.

5) Steady state flow - Water level was set equal to the peak of the two patterns considered for transient state, i.e. 6m NN and 7.3m NN respectively (Figure 2.).

Additional considerations

The mesh density in the regions where higher gradients develop was optimised (Figure S3) and constant time step of 30 min was used for both the ~1-year tide record (12,774 time steps) and the 100h storm surge.

The transient water flow analyses neglect the effect of transpiration and evapotranspiration at the embankment surface. These generate higher suction and neglecting these effects leads to a conservative estimation of the factor of safety of the slope.

Stability analysis model

The stability analysis was carried out using Bishop's simplified method (Bishop, 1955). The iterative procedure to calculate the Factor of Safety (FoS) , was completed with the module SLOPE/W. The pore-water pressures derived from the water flow analysis (either steady-state or transient-state flow) were used to calculate the shear strength and, hence, the FoS. For the transient state analysis, the pore-water pressure and, hence, the FoS, varies with time. The FoS is taken as the minimum value over the duration of the storm surge event. The Bishop method is corrected in SLOPE/W, i.e. the critical slip surface is initially assumed to be circular and then refined with the optimisation algorithm based on the segmental technique.

The equation proposed by Vanapalli, et al. (1996) was used to account for the effect of suction on shear strength (Eq. S2 in Supplemental Materials). The residual volumetric water content in

Eq. S2 was set to zero, which is appropriate for sandy and silty materials and materials with low content of clay as discussed by Tarantino & El Mountassir (2013).

Results & Discussion

Conventional versus suction-based design

The numerical analyses were aimed at comparing 'prescriptive' design based on steady-state water flow in saturated/dry embankment with 'performance-based' design based on transient-state water flow in unsaturated embankment:

- *SS-Ns (Steady-State – No suction).* Steady state water flow analysis assuming saturated condition below the phreatic surface and a virtually dry soil above the phreatic surface; shear strength criterion formulated assuming zero pore-water pressure above the phreatic surface.
- *TR-s (Transient-state –suction).* Transient state water flow analysis assuming unsaturated conditions above the phreatic surface; shear strength criterion accounting for partial saturation (Eq. [S2]).

To investigate whether and to what extent the inclination of the landside slope can be increased to raise the embankment while minimising its footprint, the FoS of the embankment was assessed for landside slopes varying from a 1:3 up to 1:1 ratio (**Table 3**). The factor of safety is expressed via the Overdesign Factor (ODF) according to the Eurocode 7:

$$ODF = \frac{R_d}{E_d} \qquad [1]$$

where E_d is the design effect of actions and R_d is the corresponding design resistance. For the case of flood embankments, and ODF equal to unity is associated with partial factors for shearing resistance $\gamma_{\varphi'}$ and effective cohesion $\gamma_{c'}$ equal to 1.25.

For each embankment geometry, the FoS was then calculated considering:

a) two types of analysis illustrated above (SS-Ns and TS-s)
b) three different foundations scenarios as shown in Figure 3 (L0, L1, and L2)
c) two hydraulic loading patterns as shown in Figure 6 (A and B)
d) two options for the shearing resistance φ’ and effective cohesion c’ of the Klei layer as per **Table 2**

Homogenous silty sand foundation (foundation scenario L0)

As an example, the results for the case of storm surge at 6m NN and landside slopes 1:3 and 1:1.25 are shown Figure 7. The conventional analysis based on steady-state water flow and saturated/dry approach is shown in Figure 7a, b for the cases c’=0 and c’≠0 respectively.

For the case c’=0, the failure surface develops through the Klei cover, fully or partially below the phreatic surface due to the high pore-water pressures developing at the toe whereas the failure surface tends to deepen into the sand core for case c’≠0 as one would expect. Under the assumption of steady-state flow and ‘dry’ soil above the phreatic surface, the landside slope 1:3 is not stable for c’=0 and an effective cohesion greater than zero is required for the Klei to make the landside slope stable. It is difficult to say whether the non-zero effective cohesion is a genuine mechanical property of the Klei or the effective cohesion is null (as the triaxial data shown in Appendix 1 seem to suggest) and c’≠0 is actually a ‘design’ value that takes into account implicitly the effect of suction effects. For avoidance of doubt, the numerical analyses are performed in parallel by considering either c’=0 or case c’≠0.

Within the conventional design approach, the landside slope is not stable when inclined 1:1.25 even if c’≠0 and the slope 1:1.25 would therefore not be allowed.

Figure 7c, d present the ODF for the case where water flow is modelled in the transient regime and the soil is assumed to be partially saturated. The phreatic surface remains well below the landside toe and the ODF increases substantially. For the 1:3 slope, the ODF increases from 0.61 to 2.22 for c'=0 and from 1.28 to 2.23 for c'≠0. The contribution of suction to shear strength makes the slope 1:1.25 stable even if c'=0.

The results presented in Figure 7 refer to storm surge pattern A (Figure 6) and the extreme landside slopes 1:3 and 1:1.25. Stability analyses were also carried out for the surge pattern B (Figure 6). Figure 8 summarises the variation of the ODF with the inclination of the landside slopes for the two design approaches (SS-Ns for steady state flow with no suction effects and TR-s for transient flow with suction effects) and the two design storm surges. The increase in peak river level (from 6m NN to 7.3m NN) produces a significant effect on the ODF if the water flow regime is analysed under steady-state conditions. For the case of storm surge 7.3 NN, the gentlest slope 1:3 is unstable even if c'≠ 0 is considered (Figure 8b).

For the case of transient flow with suction effects, the ODF remains is greater than unity and approaches unity for a landside slope angle of 45° (1:1). This inclination could also be considered a practical limit dictated by other constraints (e.g. grass mowing or other slope maintenance interventions). The increase in peak river level (from 6m NN to 7.3m NN) does not produce significant effect on the ODF if the water flow regime is analysed under transient state conditions. This is because the water front propagating from the waterside slope hardly penetrates the embankment regardless of the peak water level.

Clayey foundation (foundation scenario L1)

The upper portion of the Holocene deposit in the Hamburg harbour area, which forms the foundation of the Elbe river flood embankments, is made of alternate layers of klei and silty sand (Figure 3). The previous section has analysed the scenario of uniform foundation deposit made of silty sand. This section focuses on the case of a klei layer overlaying a silty sand layer (scenario L1 in Figure 3). The presence of a layer beneath the embankment characterised by a low hydraulic conductivity is expected to dampen down water flow underneath the flood embankment and concentrate water flow through the embankment. This scenario can potentially modify the pore-water pressure regime within the embankment and was therefore considered worth exploring.

Figure 9 shows the variation of the ODF with the inclination of the landside slopes for the two design approaches (SS-Ns for steady state flow with no suction effects and TR-s for transient flow with suction effects). For comparison, the results from the scenario L0 are reported with grey shaded symbols. For the steady-state flow analysis, the ODF reduces with respect to the foundation scenario L0 and becomes lower than unity for the storm surge 7.3 m NN even for the gentlest slope 1:3 and $c' \neq 0$ (Figure 9b). The presence of an impermeable foundation layer forces the water to flow through the embankment only and this raises the phreatic surfaces and the pore-water pressures at the landside toe of the embankment.

On the other hand, the ODF derived from the transient state analyses (TR-s) for the foundation scenario L1 is very similar to the one derived for the scenario L0. A closer inspection of the ODF curves reveals that the L1 curve lies slightly below the L0 curve for the milder slopes (18.4° and 21.8°). This is due to the fact that the phreatic surface in the L1 scenario is slightly higher and that the failure surface partially develops below the phreatic surface. On the other hand, the failure surface develops above the phreatic surface for the steeper slopes, in the region where the pore water pressure regime is only slightly affected by the change in hydraulic conductivity of the foundation, hence the ODF remains essentially the same.

Confined silty sand foundation (foundation scenario L2)

This section examines the case of silty sand layer confined by an underlying Klei layer (scenario L2 in Figure 3). The presence of a confined silty sand layer beneath the embankment is expected to promote uplift pressures at the downstream toe of the embankment.

Figure 10 shows the variation of the FoS with the inclination of the landside slopes for the two design approaches. For comparison, the results from the scenario L0 are reported with grey shaded symbols. It can be observed that there is essentially no difference between these two foundation scenarios.

Sensitivity analysis: effect of the hydraulic conductivity of the klei cover

The high ODF derived for the case where pore-water pressures are derived from transient water flow in partially saturated embankment (Figure 8, Figure 9, and Figure 10. Effect of inclination of landside slope on Overdesign Factor for the confined silty sand foundation (scenario L1). (a) 6m NN – Pattern A (b) 7.3 m NN – Pattern B (SS-Ns= steady-state flow with no suction effects; TR-s= steady-state flow with suction effects, open symbols → c'=0 and solid symbols→ c'≠0)) is associated with the low hydraulic conductivity of the Klei layer that hampers the propagation of the water front from the waterside slope (Figure 7).

The most critical soil parameter underpinning the 'performance-based' design of the Hamburg area flood embankments is therefore the hydraulic conductivity of the Klei. A sensitivity analysis was carried out to assess the influence of this parameter in the factor of safety of the flood embankment considering the variability the saturated hydraulic conductivity generally encountered in the field. The saturated hydraulic conductivity of the Klei cover was therefore increased from $k_{sat}=10^{-8}$ m/s to $k_{sat}=10^{-6}$ m/s.

The results from these analyses are presented in Figure 11 and show that even an increase in hydraulic conductivity of the Klei cover by two orders of magnitude does not decrease the ODF significantly when the stability is analysed by considering transient water flow and partial saturation. This is because the contrast between the hydraulic conductivities of the quasi-saturated Klei and the partially saturated sand core remains still remains relatively high. Under the condition of Klei cover having hydraulic conductivity two orders of magnitude lower than the design value, the maximum landside slope is 40°.

Sensitivity analysis: Rainfall effects

The high factor of safety resulting from the performance-based design is in part associated with the transient nature of the water flow through the flood embankment and in part associated with the increase in shear strength generated by the suction along the potential failure surface. A critical step in suction-based design is the evaluation of the effect of rainfall on the potential loss in suction and, hence, shear strength. For this reason, the factor of safety for the foundation scenario L0 was assessed assuming that i) a rainfall occurs at the same time and for the same duration as the storm surge and ii) an antecedent rainfall of 30 days occurs before the storm surge.

Figure 12 reports the precipitation statistics of rainfall events in Hamburg over the observation period 1997-2014 (17 years). The red dotted curve shows the maximum cumulated rainfall recorded over a duration given by the 'aggregation time'. For example, a cumulative rainfall of 97 mm is associated with an aggregation time of 100h. This means that the maximum cumulated rainfall recorded over a time window of 100h over the 17 year-period is equal to 97 mm. The blue dotted curve represents the same cumulative rainfall versus aggregation time associated with a return period of 100 years (99 percentile).

Two rainfall events were considered. The first consists of 97 mm over 100h, consistent with the maximum cumulative rainfall recorded over the aggregation time of 100h in the 17 year-period (Figure 12) and occurring at the same time as the storm surge (see Figure 6). The second event consists of 261 mm over 30 days, it initiates before the storm surge and ends when the storm surge ends. These two rainfall events are 'extreme' in the sense that they are associated with a return period >100 years.

Figure 13 shows the ODF for the foundation scenario L0 and storm surge pattern 7.3m NN for the cases of rainfalls of 97mm/100h and 261 mm/30d. The ODF is compared with the ODF in the absence of rainfall (shaded gray triangles). The ODF decreases but only marginally for both rainfall events. The reason why the rainfall events do not cause a significant drop in suction is that most of the rainfall tends to run off once pore water pressure increases up to zero at the boundary. Under the condition of concomitant or antecedent rainfall, the maximum landside slope is 43°.

Economic and environmental implications of prescriptive and performance-based design

Land expropriation

Figure 14a shows the case where the flood embankment is raised from 5m to 7m without changing its footprint. This would result in a landside slope 1:1.3 (37°) that would still allow for a ODF greater than 1 if the embankment is designed by assuming transient water flow and partial saturation (Figure 8 to Figure 11, Figure 13). Compared with the prescriptive design where the landside slope is maintained 1:3, this would allow for a footprint saving of 12 m^2 per linear meter of embankment and volume saving of 42 m^3 per linear meter of embankment. If a new embankment must be built with a landside slope 1:1.2 (40°), the footprint saving would be 13 m^2 per linear meter of embankment and volume 45.5 m^3 per linear meter of embankment (Figure 14b).

A survey of land values on real estate market in Hamburg reveals that, at the time of writing, the price of land with building permits is around €250-400/m^2 in the harbour area and Wilhelmsburg island on the south side of the river Elbe (LBS, 2020). Assuming an average price of land of €325/m^2, the saving of expropriation cost moving from the prescriptive design (SS-Ns) to the performance-based design (TR-s) would therefore be €3.9M/km for the flood embankment retrofit and €4.5M/km for a new embankment.

Habitat suppression

The retrofit of the flood embankment using the performance-based design (Figure 14a) could be achieved with no habitat suppression compared to the prescriptive design that would cost at least 1.2 ha per linear km of compensatory habitat to be restored somewhere else. It should be noted that habitat compensation need to take into account not only direct loss due to the portion of land covered by the upgraded flood embankment but also indirect losses due to the time required to restore the ecological function of the adjacent habitat that will be damaged during the construction period (Esteves and Thomas, 2014).

If a new flood embankment must be built, the habitat to be compensated for the case of the performance-based designed flood embankment would be limited to 3.1ha per linear km compared to the traditional prescriptive-based design that would require 3.8ha per linear kilometre of compensatory habitat.

Embodied carbon savings

A full Life Cycle Analysis (LCA) should be developed (Glass 2013) for an accurate quantification of the embodied carbon savings associated with the performance-based design in comparison with the conventional prescriptive design. However, a LCA is out of the scope of this work and a simplified approach was pursued to estimate the order of magnitude of the carbon that can be saved by the performance-based design proposed. The embodied carbon per unit volume of embankment was estimated on the basis of the data available for the Cobbins Brook flood embankment that present characteristics similar to the flood embankments in the Hamburg area as discussed in Appendix II. The computation of the overall carbon emission for the Cobbins Brook flood alleviation scheme led to an embodied carbon between 64-84 kg of CO_2e/m^3.

The volume saved by the performance-based design was found to be equal to 42,000 m^3/km for the retrofitted embankment (Figure 14a) and 46,000 m^3/km for a new embankment (Figure 14b). If this volume is multiplied by the estimated embodied carbon (64-84 kg of CO_2e/m^3), the carbon saving would result in 2,678-3,525 tCO_2e/km for the retrofitted embankment and 3,125-4,113 tCO_2e/km for a newly built, which roughly corresponds to 12.5-16.8 million car/km or more than 3700-5000 flights London-New York/km. These figures are significant if one considers that earthen flood-protection infrastructure in the Hamburg area extends over 130 km.

Conclusions

The paper has discussed the problem of retrofitting flood embankments in a climatic-change scenario by raising their crest with reference to the case of the Elbe River in Hamburg. If the embankments are raised by maintaining the same 'prescriptive' landside slope, the cost in terms of land expropriation, habitat compensation, and embodied carbon would be significantly high.

The paper has made the case that performance-based design based on transient water flow analysis and accounting for the partial saturation of the embankments can lead to substantial economic and environmental saving compared to the tradition prescriptive design, which is based on steady-state flow analysis and the assumption that the soil above the phreatic surface is dry.

To demonstrate the differences between prescriptive and performance-based design, the landside slope was varied from the prescriptive value of 1:3 up to 1:1, which might be considered an upper limit of the landside slope dictated by maintenance operations. It has been shown that design based on transient water flow and partial saturation (performance-based design) allows for the landside slope to be increased potentially up to 1:1 still maintaining the Overdesign Factor (ODF) substantially greater than the one derived from traditional analysis (steady-state water flow and saturated/dry approach).

The high factor of safety resulting from the performance-based design is in part associated with the transient nature of the water flow through the flood embankment (the water front propagating from the riverside slope hardly penetrates the embankment) and in part associated with the increase in shear strength generated by the suction along the potential failure surface.

The performance-based design would allow the embankment to be raised without increasing its footprint (in contrast with the prescriptive design where the raising of the crest is achieved at the expenses of significant increase in embankment footprint). In the Hamburg area, this would allow savings expropriation cost of the order of €3.9M per linear kilometre and carbon savings of the order of 2600-3500 tCO_2 per linear kilometre.

The suction-based design of flood embankments relies on the low (unsaturated) hydraulic conductivity of the embankment materials, and this poses a challenge in practice due to the difficulty associated with the reliable characterisation the hydraulic properties of the embankment geomaterials and their potential degradation over time (e.g. effect of drying and wetting cycles, fine fissuring and/or surface cracks). Suction-based design of flood embankments would therefore require an additional investment in terms of laboratory and field characterisation of unsaturated hydraulic conductivity of embankment materials and possibly low-cost field monitoring. This paper aimed at demonstrating that such an additional investment could be worthwhile in the light of the economic, carbon, and environmental savings enabled by the suction-based design.

Data Availability Statement

All data, models, or code that support the findings of this study are available from the corresponding author upon reasonable request.

Acknowledgements

The authors wish to acknowledge the support of the European Commission via the Marie Skłodowska-Curie Innovative Training Networks (ITN-ETN) project TERRE 'Training Engineers and Researchers to Rethink geotechnical Engineering for a low carbon future’ (H2020-MSCA-ITN-2015-675762).

APPENDIX 1 – KLEI SHEAR STRENGTH PARAMETERS

The Hamburg Geological Survey made available a database of hydraulic and mechanical properties of the soils in the Hamburg area (GLH, 2017). Shear strength data for klei are provided via two datasets including Consolidate-Drained (CD) and Consolidated-Undrained (CU) triaxial data tests. As shown in Figure 15, the two datasets are not very consistent. It is not surprising that shear strength at relatively high stresses can be represented by either a relatively high friction angle ϕ' and zero effective cohesion ($c'=0$) or a lower friction angle and $c'>0$. However, the values of friction angle would have been expected to be similar (at similar effective cohesion values).

When predicting shear strength at relatively high stresses, the combination of high friction angle ϕ' and zero effective cohesion ($c'=0$) and the combination of lower friction angle and $c'>0$ can be considered equivalent. This is not the case at low stresses because even a small cohesive term in the shear strength criterion can radically change the results of a stability analysis.

Two options were considered. The values of friction angle ϕ' and effective cohesion c' from Figure 15a were plotted as in Fi*gure 16*. As expected, the friction angle decreases with effective cohesion. As per option 1, the Klei effective cohesion was set equal to its average value ($c'=7.7$ kPa) and the friction angle derived from the linear correlation as shown in Fi*gure 16* ($\phi'=27.4°$).

The raw data available from the Triaxial-CU dataset reported in the Hamburg Geological Survey database (GLH, 2017) were also re-interpreted (i.e. specimens 6 and 7 in Figure 15b). As shown in Figure 17, the triaxial stress path seem to be satisfactorily enveloped by a straight line passing through the origin, i.e. the Klei seems to show zero effective cohesion. This is further supported by the finding of Quast (1977, pages 134-136).

As shown in Figure 15a, the value of the friction angle associated with zero effective cohesion is ϕ'=30° and this value was adopted in the analysis. However, it should be noted that the null effective cohesion exhibited by the two samples in Figure 17 could just be an artefact of sampling disturbance.

APPENDIX 2 – EMBODIED CARBON FOR COBBINS BROOK EMBANKMENT

The Cobbins Brook flood alleviation scheme protects the town of Waltham Abbey in Essex UK and a 1.3 Million Flood Storage Reservoir (FSR) located 2km upstream of Waltham Abbey was constructed in 2009. The earth dam has a maximum height of 7.5m, length of 750 m with 1:3 slopes on both sides except for the 1:6 slope of the spillway on the landside slope. The embankment has been fully constructed using nearby won London Clay compacted to an optimum water content of 21.5% to achieve a maximum air voids of ~5%. Considering the water content and porosity of the compacted materials as reported by Lee et al (2010) and a specific gravity for London Clay of 2.7 according to Monroy et al (2010), the density of the as-compacted material can be estimated in the range 1971-2075 kg/m3 with an average value of 2023 kg/m^3.

The carbon footprint associated with the construction phase of the Cobbins Brook flood alleviation scheme has been assessed by Defra (2010). In particular, Table A4.22 of the Defra report lists the tonnes of CO_2 generated for each material and task during the construction phase. The items that are relevant to the flood embankment in the Hamburg area are listed in the table below, with the exception of the item 'Quarried Material (clay + aggregates)' that has been added.

The carbon associated with this item appeared to be out of range (probably miscalculated) and was estimated differently. The embodied carbon associated with the quarried material was assumed to be equal to 0.024 tCO_2 per tonne according to the ICE V3 database (Hammond, 2008) and multiplied by the mass of material forming the Cobbins Brook flood embankment. In turn this mass was estimated in two independent ways:

i) using the information directly provided by Defra (2010) about the mass of material used to construct the embankment, i.e. 152,000t of clay and 8,300t of aggregates. This leads to a carbon contribution for the quarried material of 3847 tCO_2.

ii) using the information provided by Lee (2010) about the volume of embankment (~ 56000 m^3) and the estimated bulk density of 2023 kg/m^3 as shown above. This leads to a carbon contribution for the quarried material of 2718 tCO2.

The computation of the overall carbon emission for the Cobbins Brook flood alleviation scheme during the construction phase is reported in Table 4. By dividing the total carbon emission for the Cobbins Brook embankment by its volume (56,000 m3), the embodied carbon of a flood embankment can be estimated between 64-84 kg of CO2e/m3.

SUPPLEMENTAL MATERIALS

Equation S1 – Water flow equation

$$\frac{\partial}{\partial x}\left[k\frac{\partial}{\partial x}\left(\frac{u_w}{\gamma_w}+z\right)\right]+\frac{\partial}{\partial z}\left[k\frac{\partial}{\partial z}\left(\frac{u_w}{\gamma_w}+z\right)\right]=\frac{\partial\theta}{\partial u_w}\frac{\partial u_w}{\partial t} \qquad \text{[S1]}$$

x = horizontal coordinate

z = elevation,

u_w = pore-water pressure,

γ_w = unit weight of water,

θ = volumetric water content,

k = hydraulic conductivity (assumed to be isotropic)

t = the time

Equation S2 – Shear strength equation

$$\tau = \left(\sigma + s\frac{\theta - \theta_r}{\theta_s - \theta_r}\right)\tan\phi' \qquad [S2]$$

τ = shear strength

σ = normal stress

s = suction

θ = volumetric water content

θ_{sat} = saturated volumetric water content,

ϕ' = friction angle.

References

Baets, S. D., Torri, D., Poesen, J., Salvador, M. P., & Meersmans, J. (2008). Modelling increased soil cohesion due to roots with EUROSEM. Earth Surface Processes and Landforms: The Journal of the British Geomorphological Research Group, 33(13), 1948-1963.

Baral S. Wang JX, Alam S. and Patterson WB (2019). Experimental and Analytical Studies on the Root Reinforcement Effect of a Grass Species, Spartina alterniflora. Eighth International Conference on Case Histories in Geotechnical Engineering

Barnard, P.L., Erikson, L.H., Foxgrover, A.C. J.A. Finzi Hart, P. Limber, A.C. O’Neill, M. van Ormondt, S. Vitousek, N. Wood, M.K. Hayden & J.M. Jones (2019). Dynamic flood modeling essential to assess the coastal impacts of climate change. *Sci Rep* **9,** 4309. DOI: 10.1038/s41598-019-40742-z.

Bhaskar, P., Puppala, A. J., & Boluk, B. (2022). Influence of Unsaturated Hydraulic Properties on Transient Seepage and Stability Analysis of an Earthen Dam. International Journal of Geomechanics, 22(7), 04022105.

Bishop, A. W. (1955). The use of the slip circle in the stability analysis of slopes. Geotechnique, 5(1), 7-17.

Comino, E., Marengo, P., & Rolli, V. (2010). Root reinforcement effect of different grass species: A comparison between experimental and models results. Soil and Tillage research, 110(1), 60-68.

Committee for coastal protection works of the German Society for Earthworks and Foundation Engineering and the Society for Port Engineering (Ausschuss für Küstenschutzwerke der Deutschen Gesellschaft für Erd- und Grundbau und der Hafenbautechnischen Gesellschaft) (2020). Recommendations B 2002 - Geotechnical investigations of sea and tidal current dike (Empfehlungen B 2002 - Geotechnische Untersuchungen von See- und Tidestromdeichen). In: Die Küste 88. Karlsruhe: Bundesanstalt für Wasserbau. S. 303-337.

Committee on Climate Change (2013) Managing the land in a changing climate. Adaptation Sub-Committee Progress Report 2013. Committee on Climate Change, London

Department for Environment, Food and Rural Affairs (Defra) (2002). Directing the Flow: Priorities for Future Water Policy. Department for Environment, Food and Rural Affairs, Defra Publications (http://www.defra.gov.uk).

Esteves, L. S., & Thomas, K. (2014). Managed realignment in practice in the UK: Results from two independent surveys. Journal of Coastal Research, Special Issue, 70, 407–413.

GeoSlope (2019) Seepage modelling with SEEP/W 2012 – An engineering methodology, 4th Ed., GeoSlope International, Alberta, Canada

Glass, J., Dyer, T., Georgopoulos, C., Goodier, C., Paine, K., Parry, T., ... & Gluch, P. (2013). Future use of life-cycle assessment in civil engineering. Proceedings of the Institution of Civil Engineers-Construction Materials, 166(4), 204-212.

GLH (2017). Geologisches Landesamt Hamburg, http://ingdata.hamburg.de/ (last accessed 01/06/2020)

Gragnano, C. G., Rocchi, I., & Gottardi, G. (2021). Field Monitoring and Laboratory Testing for an Integrated Modeling of River Embankments under Transient Conditions. Journal of Geotechnical and Geoenvironmental Engineering, 147(9), 05021006.

Hammond, G. P., & Jones, C. I. (2008). Embodied energy and carbon in construction materials. Proceedings of the Institution of Civil Engineers-Energy, 161(2), 87-98.

HPA (2008). Technische Rahmenbedingungen (TR HWS-Bau). Hamburg Port Authority.

Johari, A., & Talebi, A. (2019). Stochastic analysis of rainfall-induced slope instability and steady-state seepage flow using random finite-element method. International Journal of Geomechanics, 19(8), 04019085.

Khalilzad, M., Gabr, M. A., & Hynes, M. E. (2015). Deformation-based limit state analysis of embankment dams including geometry and water level effects. International Journal of Geomechanics, 15(5), 04014086.

Lee, S., Cass, J., Cornick, S., & Bradley, M. (2010). Cobbins Brook Flood Storage Reservoir. In Managing dams Challenges in a time of change (pp. 364-375). Thomas Telford Ltd.

LBS (2020). Immobilien markt atlas 2020 Hamburg und Umland. https://www.lbs.de/unternehmen/schleswig_holstein_hamburg_6/regionales_thema_68/regionales_thema_63.jsp (last accessed 01/06/2020)

Lu, N. And. Likos, W.J. (2004). Unsaturated Soil Mechanics. Wiley.

Ngo, P. S. N., Garciano, L. E. O., De Leon, M. P., Lopez, N. S. A., Ishii, H., Iimura, K., ... & Shibayama, T. (2022). Experimental and Numerical Modeling of a Tide Embankment Section Subjected to Storm Surge in Tacloban City, Philippines. Natural Hazards Review, 23(4), 05022007.

Quast, P.: Ein Beitrag zum Kriechverhalten eines norddeut-schen Kleis, Mitteilungen des Lehrstuhls für Grundbau,Bodenmechanik und Energiewasserbau der TU Hannover,Heft 11, 1977

Showkat, R., Mohammadi, H., Babu, G. S., & ASCE, F. (2022). Effect of Rainfall Infiltration on the Stability of Compacted Embankments. International Journal of Geomechanics, 22(7).

Spalding, M. D., Ruffo, S., Lacambra, C., Meliane, I., Hale, L. Z., Shepard, C. C., & Beck, M. W. (2014). The role of ecosystems in coastal protection: Adapting to climate change and coastal hazards. Ocean & Coastal Management, 90, 50-57.

Spencer, K. L., & Harvey, G. L. (2012). Understanding system disturbance and ecosystem services in restored saltmarshes: integrating physical and biogeochemical processes. Estuarine, Coastal and Shelf Science, 106, 23-32.

Stubbs, B. (2008). Plain English guide to sustainable construction. Construction-Excellence in the Built Environment. Available at: https://constructingexcellence.org.uk/wp-content/uploads/2015/02/SUSTAINGUIDE.pdf accessed 8/7/2020.

Sundseth, K. (2012). The EU Birds and Habitats Directives. European Commission, Environment Directorate General

Tarantino A. & El Mountassir G. (2013). Making unsaturated soil mechanics accessible for engineers: Preliminary hydraulic–mechanical characterisation & stability assessment Engineering Geology, 165: 89-104

Tarantino A. (2010). Basic concepts in the mechanics and hydraulics of unsaturated geomaterials. In: L. Laloui (Ed.), Mechanics of Unsaturated Geomaterials, pp. 1-23. Wiley.

Tarantino, A. & Di Donna, A. (2019). Mechanics of unsaturated soils: simple approaches for routine engineering practice. Italian Geotechnical Journal, 4/2019: 6-46.

Vahedifard, F., Jasim, F. H., Tracy, F. T., Abdollahi, M., Alborzi, A., & AghaKouchak, A. (2020). Levee fragility behavior under projected future flooding in a warming climate. Journal of Geotechnical and Geoenvironmental Engineering, 146(12).

van Genuchten, M. T. (1980). A closed- form equation for predicting the hydraulic conductivity of unsaturated soils. Soil science society of America journal, 44(5), 892-898.

von Storch, H., Meinke, I., & Claußen, M. (2017). Hamburger Klimabericht–Wissen über Klima, Klimawandel und Auswirkungen in Hamburg und Norddeutschland (p. 302). Springer Nature.

Vanapalli, S. K., Fredlund, D. G., Pufahl, D. E., & Clifton, A. W. (1996). Model for the prediction of shear strength with respect to soil suction. Canadian geotechnical journal, 33(3), 379-392.

Vousdoukas, M., Mentaschi, L. & Voukouvalas, E., Verlaan, M. & Feyen, L. (2017). Extreme sea levels on the rise along Europe's coasts. Earth's Future, 5: 304–323. DOI: 10.1002/2016EF000505.

Weder, C., Müller, G., & Brümmer, B. (2017). Precipitation extremes on time scales from minute to month measured at the Hamburg Weather Mast 1997-2014 and their relation to synoptic weather types. Meteorologische Zeitschrift, 26, 507-524.

Zhang, Z., Fu, X., Sheng, Q., Du, Y., Zhou, Y., & Huang, J. (2021). Stability of cracking deposit slope considering parameter deterioration subjected to rainfall. International Journal of Geomechanics, 21(7), 05021001.

Table 1. van Genuchten parameters of water retention and hydraulic conductivity functions

Material	**D_{80} [mm]**	**s_{AEV} (empirical) [kPa]**	**α [kPa^{-1}]**	**n [-]**	**k_{sat} [m/s]**
Klei	0.035	44	0.010	1.7	1e-8
Silty Sand	0.4	5	0.100	2	1e-6
Clean Sand	1	4	0.142	3	1e-5

Table 2. *Mechanical parameters*

Material	γ_{dry} [kN/m^3]	γ_{sat} [kN/m^3]	ϕ’ (°)	c' [kPa]
Klei top layer (200 mm) – option 1	12.5	17.5	27.4	11.7
Klei top layer (200 mm) – option 2			30	4
Klei – option 1	12.5	17.5	27.4	7.7
Klei – option 2			30	0
Sand	17	20	36	0
Silty Sand	18	20	33	0

Table 3. *Landslide slopes examined*

H:L slope ratio	1:3.00	1:2.50	1:2.00	1:1.75	1:1.50	1:1.25	1:1.00
Slope Angle [°]	18.4	21.8	26.6	29.7	33.7	38.7	45.0

*Table 4 Carbon emission during construction of the Cobbins Brook embankment. The contribution of quarried material is re-calculated with two different approaches: *the amount of quarried material reported by DEFRA/EA (2010) is multiplied by the carbon factor for soil in Hammond (2008), ** the mass of won clay is calculated from the volume and density provided by Lee (2010) and then multiplied by the same carbon factor.*

<table>
<tr><th>Subtotal</th><th>CO_2 tonnes</th><th>CO_2 tonnes</th></tr>
<tr><td>Quarried Material (clay + aggregates)</td><td>3847*</td><td>2718**</td></tr>
<tr><td>Material Transport</td><td colspan="2">424</td></tr>
<tr><td>Plant Emissions</td><td colspan="2">344</td></tr>
<tr><td>Personnel Travel</td><td colspan="2">36</td></tr>
<tr><td>Portakabins</td><td colspan="2">19</td></tr>
<tr><td>Timber</td><td colspan="2">19</td></tr>
<tr><td>Waste Removal</td><td colspan="2">7</td></tr>
<tr><td>Miscellaneous</td><td colspan="2">4</td></tr>
<tr><td>Total</td><td>4700</td><td>3571</td></tr>
</table>

Climate change adaptation of Elbe River flood embankments via suction-based design

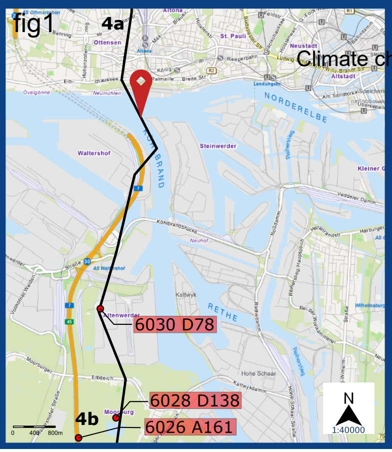

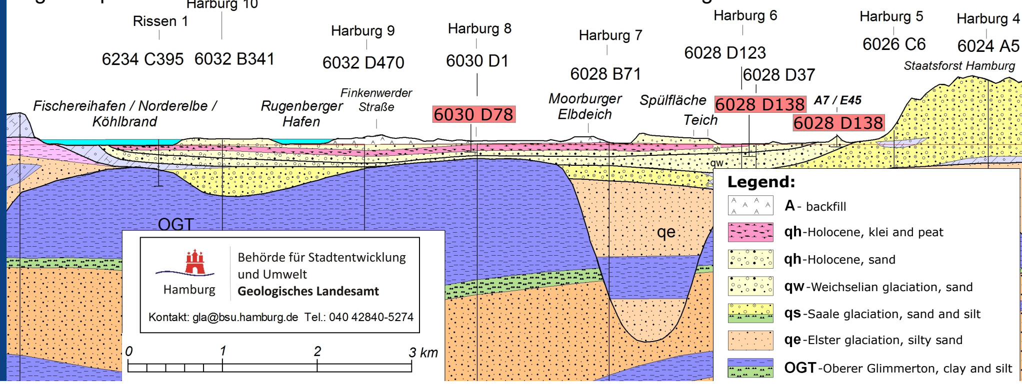

Representative boreholes of the uppermost layers

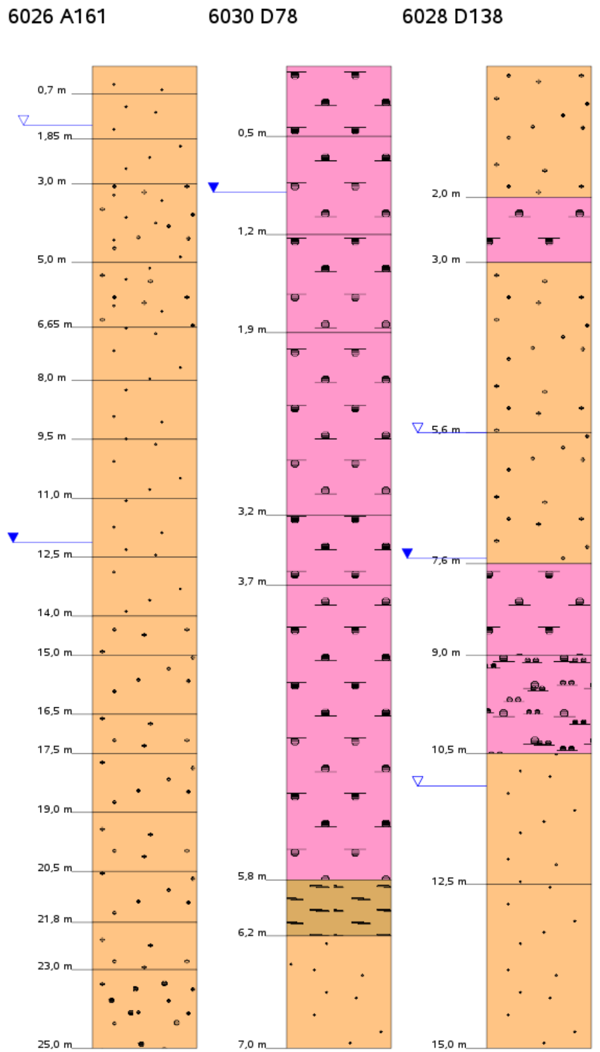

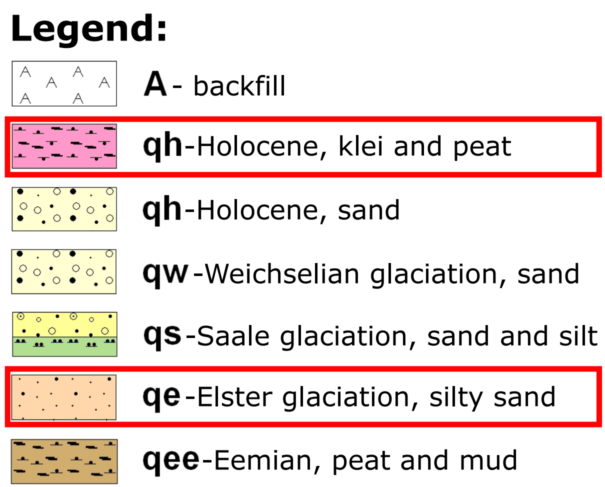

Scenario	Borehole	Location (EPSG:3857) est-X [m]	north-Y [m]
L0	**6026 A161**	1103987	7071225
L1	**6030 D78**	1104416	7077318
L2	**6028 D138**	1104583	7073446

fig2

Click here to access/download;Figure;Fig2.pdf

Climate change adaptation of Elbe River flood embankments via suction-based design

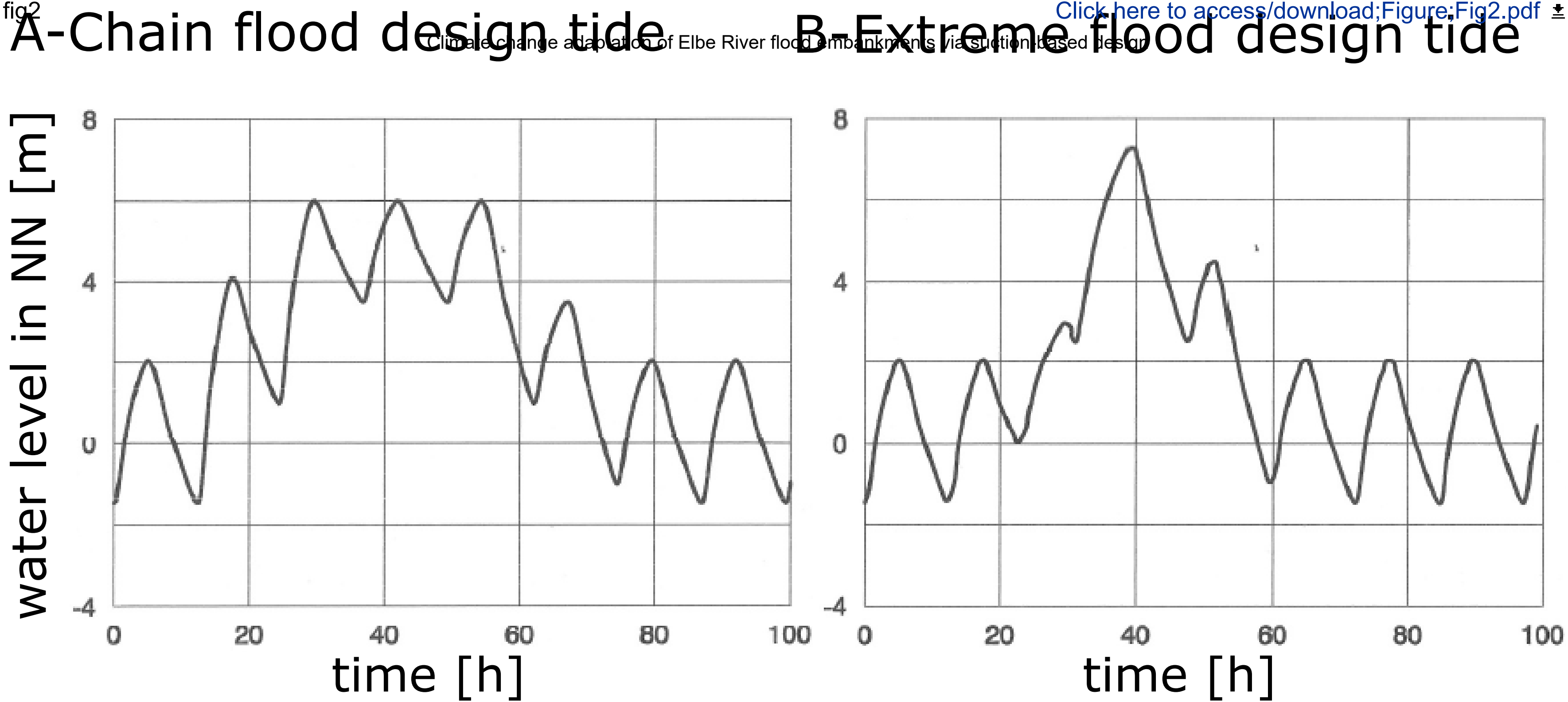

fig3

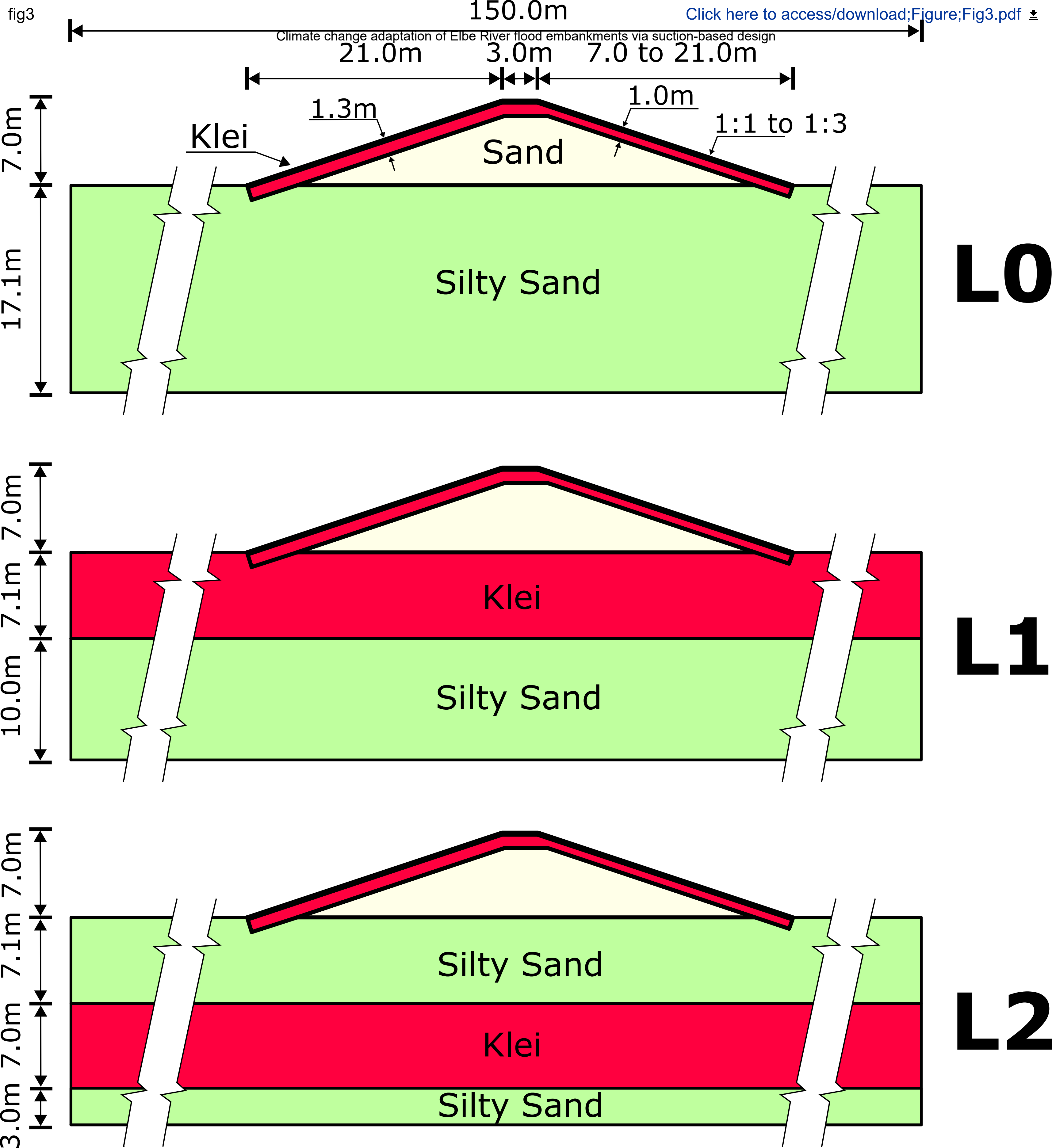
150.0m
21.0m
3.0m
7.0 to 21.0m
1.3m
1.0m
1:1 to 1:3
Klei
Sand
Silty Sand
7.0m
17.1m
L0
7.0m
7.1m
10.0m
Klei
Silty Sand
L1
7.0m
7.1m
7.0m
3.0m
Silty Sand
Klei
Silty Sand
L2

fig4

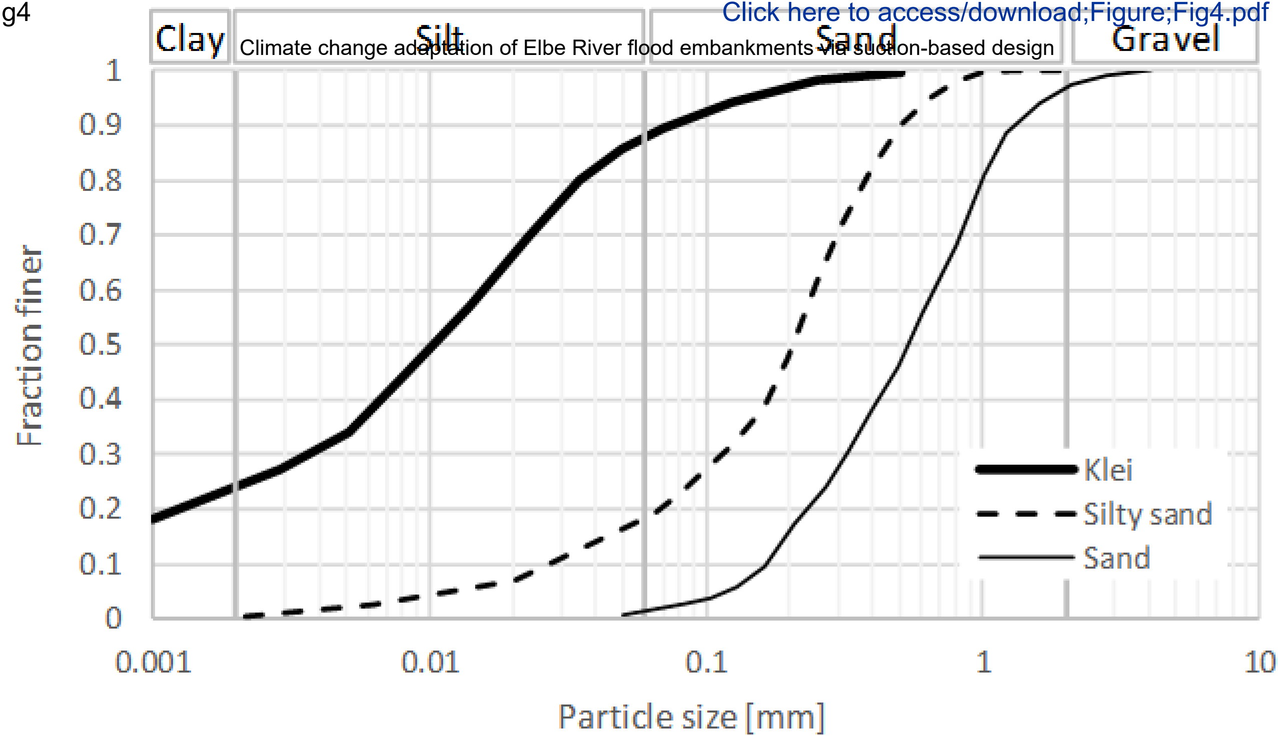
Clay
Silt
Sand
Gravel
1
0.9
0.8
0.7
0.6
0.5
0.4
0.3
0.2
0.1
0
Fraction finer
0.001
0.01
0.1
1
10
Particle size [mm]
Klei
Silty sand
Sand

Climate change adaptation of Elbe River flood embankments via suction-based design

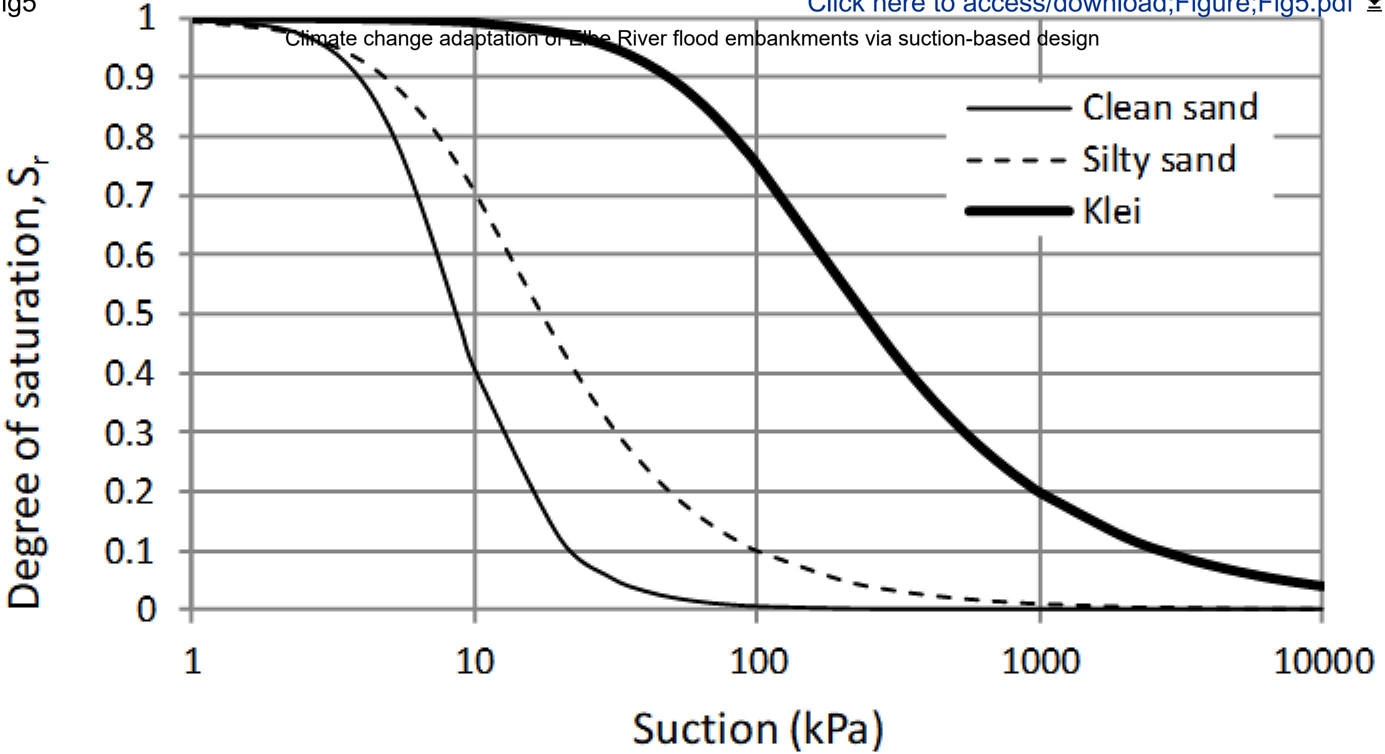

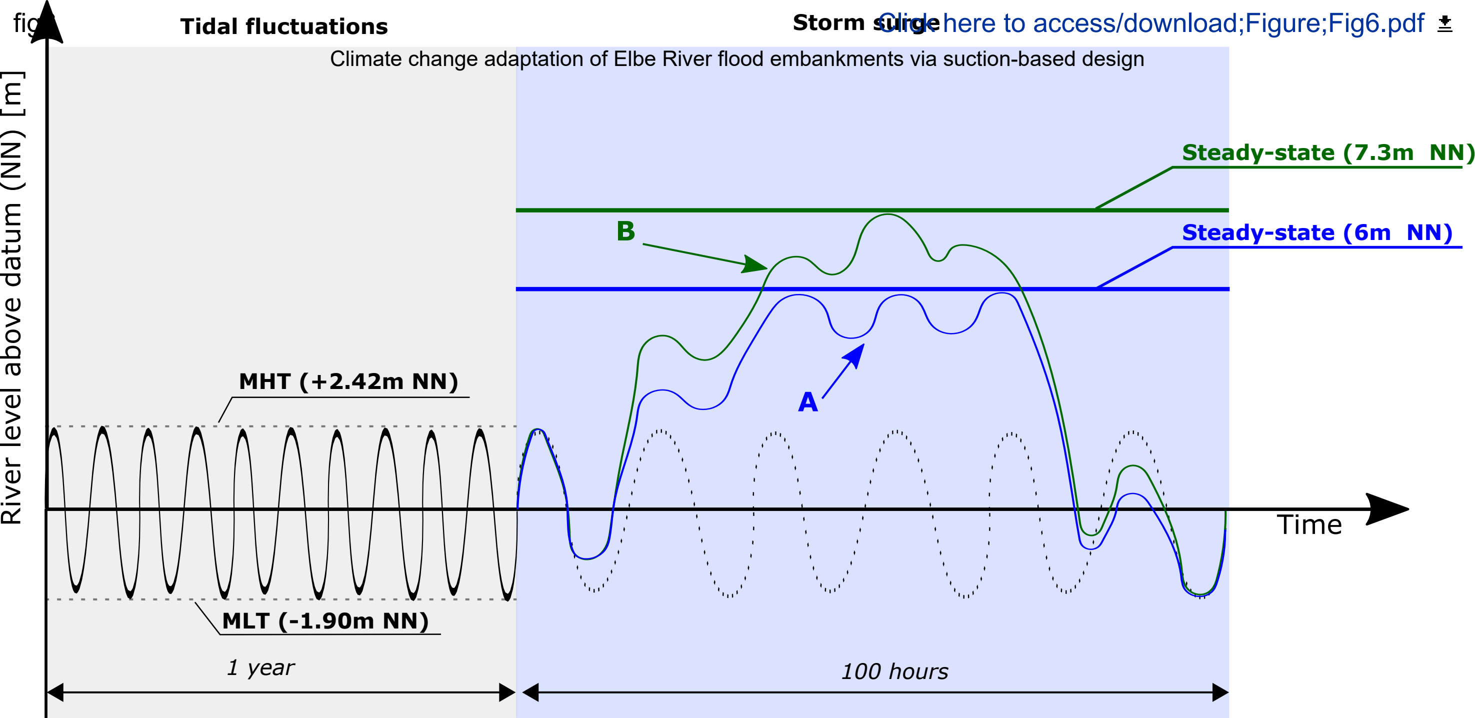
fig
Tidal fluctuations
Storm surge
Steady-state (7.3m NN)
Steady-state (6m NN)
B
A
MHT (+2.42m NN)
MLT (-1.90m NN)
River level above datum (NN) [m]
Time
1 year
100 hours

Fig7

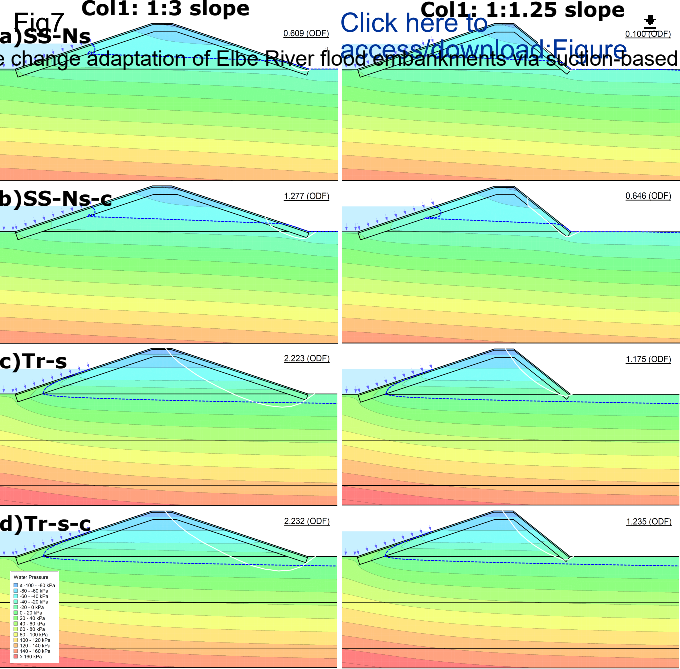
Col1: 1:3 slope
Col1: 1:1.25 slope
a)SS-Ns
0.609 (ODF)
0.100 (ODF)
b)SS-Ns-c
1.277 (ODF)
0.646 (ODF)
c)Tr-s
2.223 (ODF)
1.175 (ODF)
d)Tr-s-c
2.232 (ODF)
1.235 (ODF)
Water Pressure
≤ -100 - -80 kPa
-80 - -60 kPa
-60 - -40 kPa
-40 - -20 kPa
-20 - 0 kPa
0 - 20 kPa
20 - 40 kPa
40 - 60 kPa
60 - 80 kPa
80 - 100 kPa
100 - 120 kPa
120 - 140 kPa
140 - 160 kPa
≥ 160 kPa

fig8

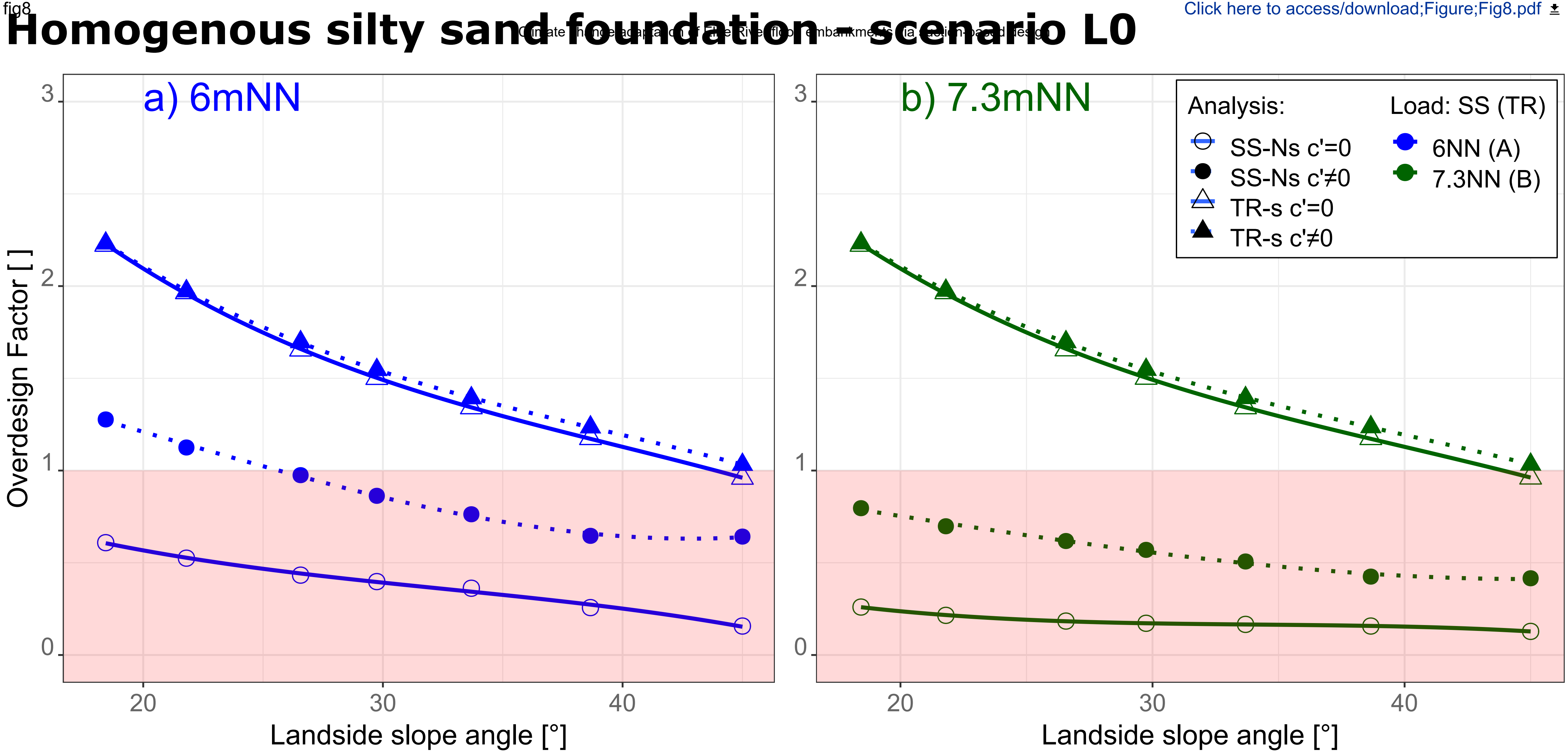
Homogenous silty sand foundation - scenario L0
a) 6mNN
b) 7.3mNN
Overdesign Factor [ ]
Landside slope angle [°]
Landside slope angle [°]
Analysis:
SS-Ns c'=0
SS-Ns c'≠0
TR-s c'=0
TR-s c'≠0
Load: SS (TR)
6NN (A)
7.3NN (B)
0
1
2
3
0
1
2
3
20
30
40
20
30
40

Clayey foundation - scenario L1

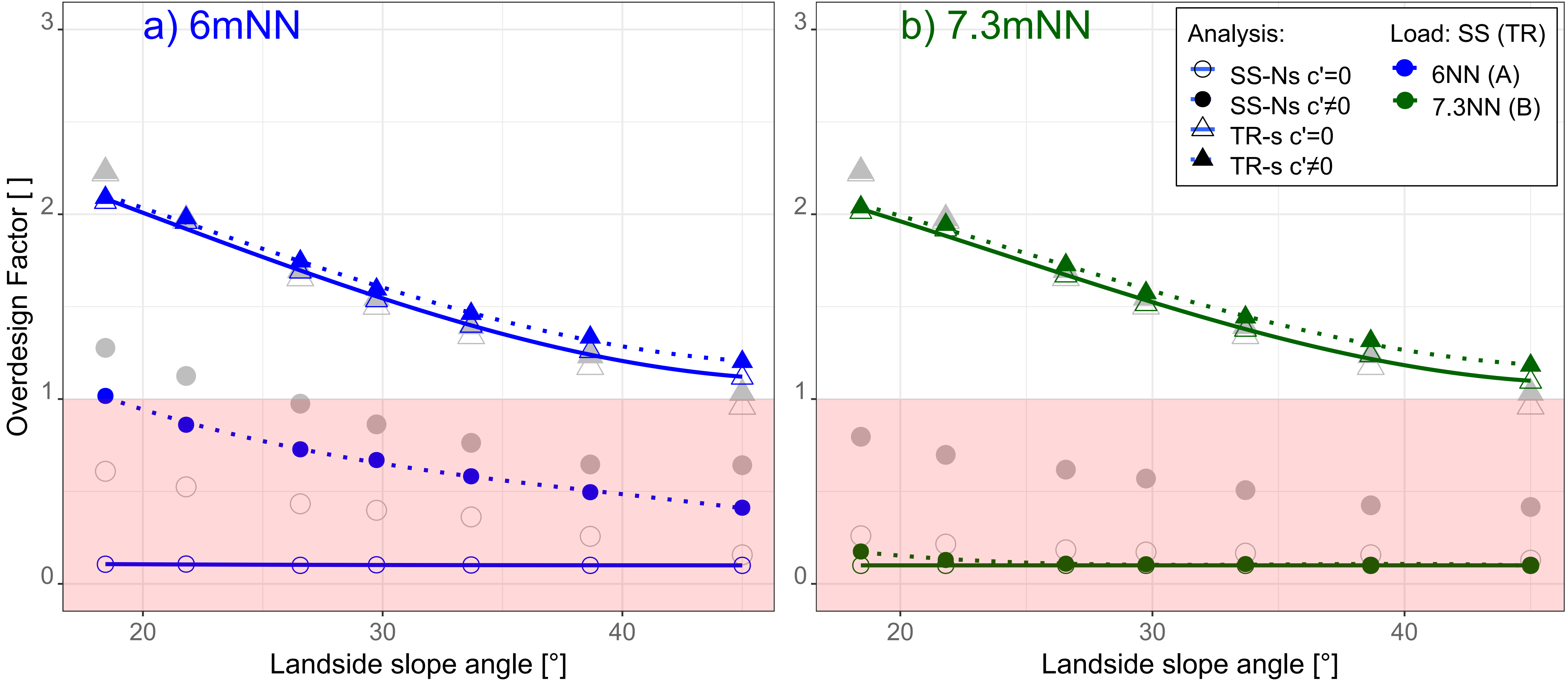

Confined silty sand foundation - scenario L2

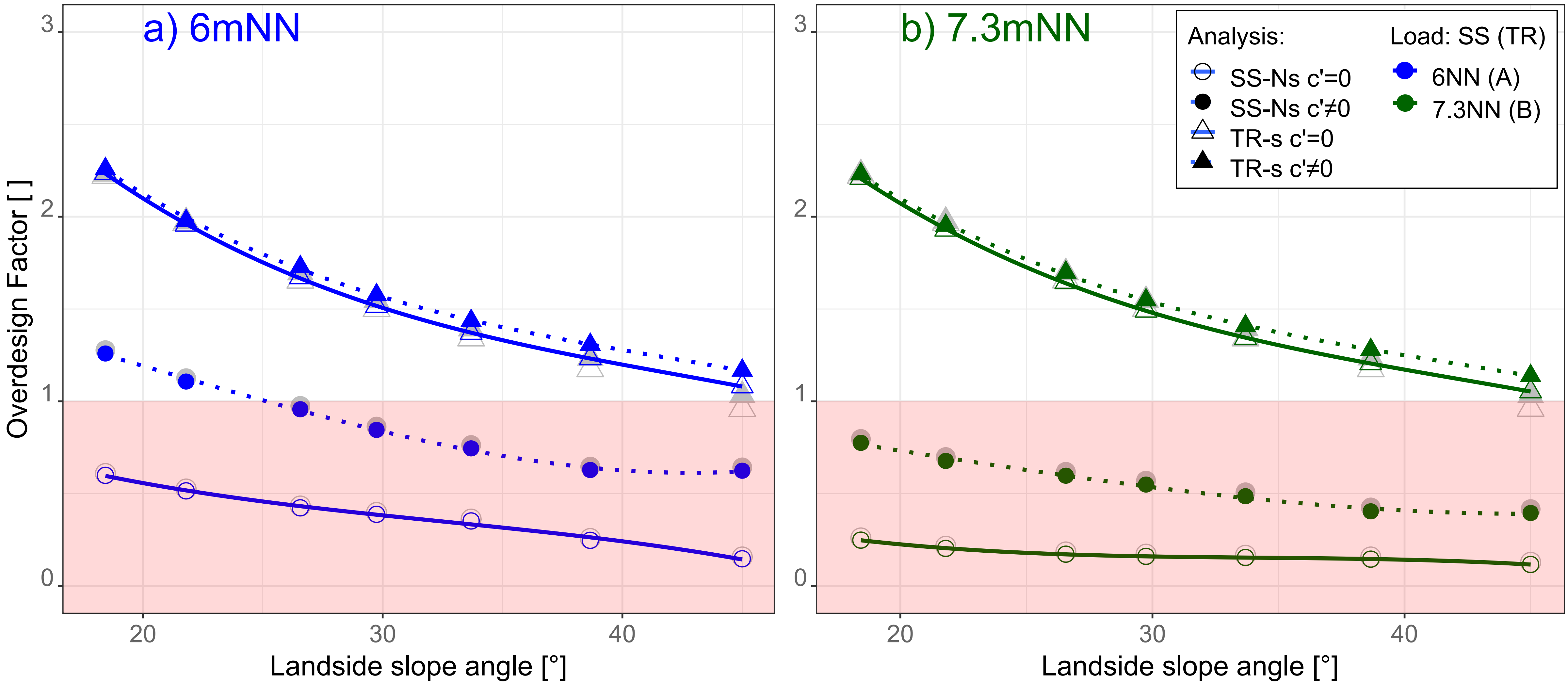

Hydraulic conductivity of klei cover $k_{sat} = 10^{-6} m/s$ - scenario L0

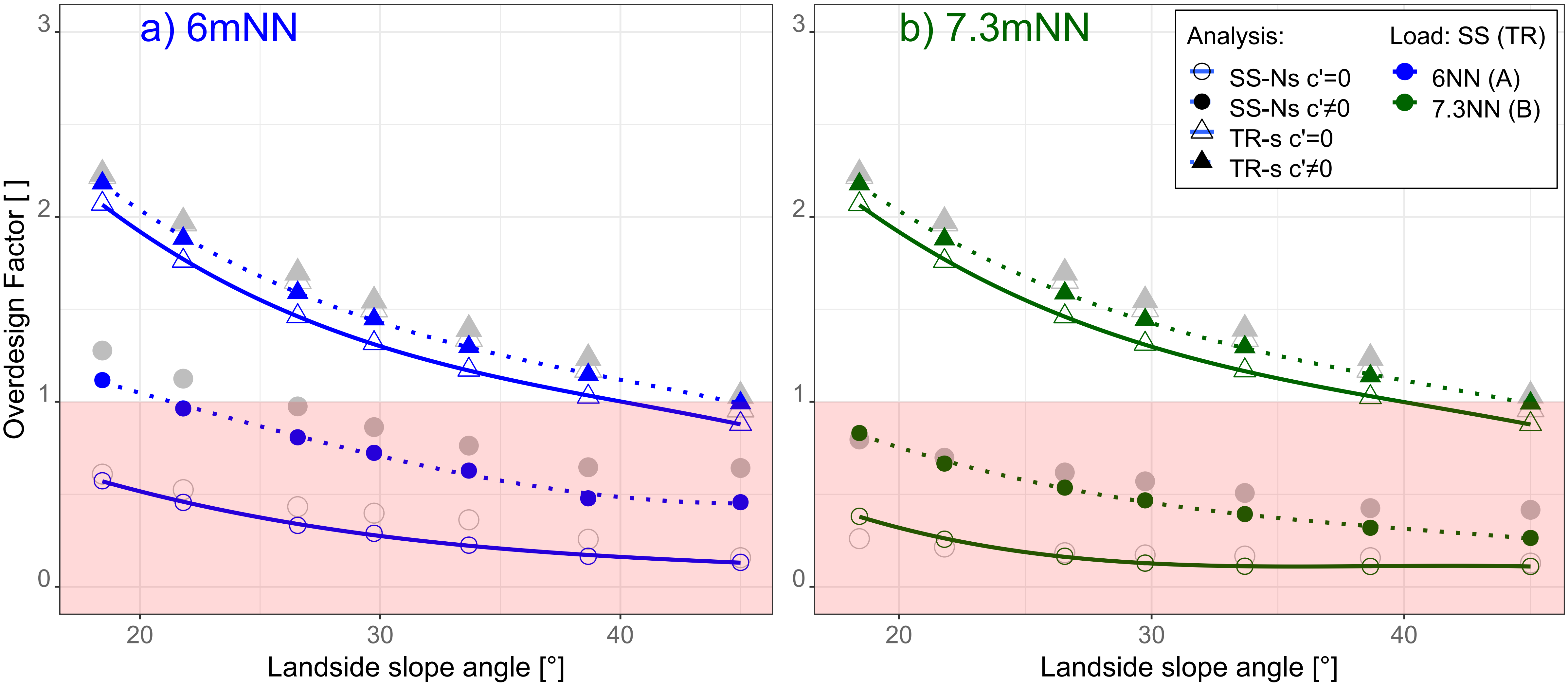

fig12

Click here to access/download;Figu

change adaptation of Elbe River flood embankments via suction-base

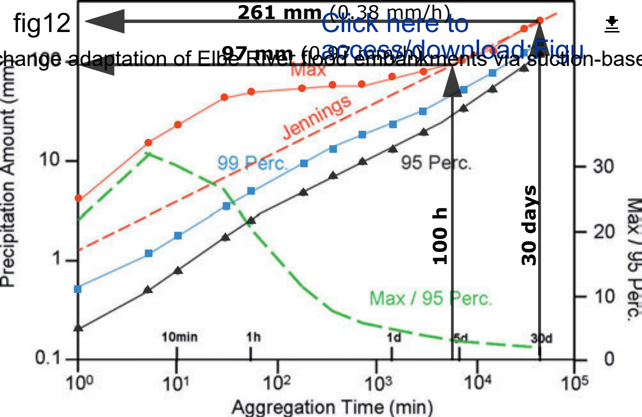

Rainfall effects for q_{in}=0.97mm/h & q_{in}=0.38mm/h - scenario L0

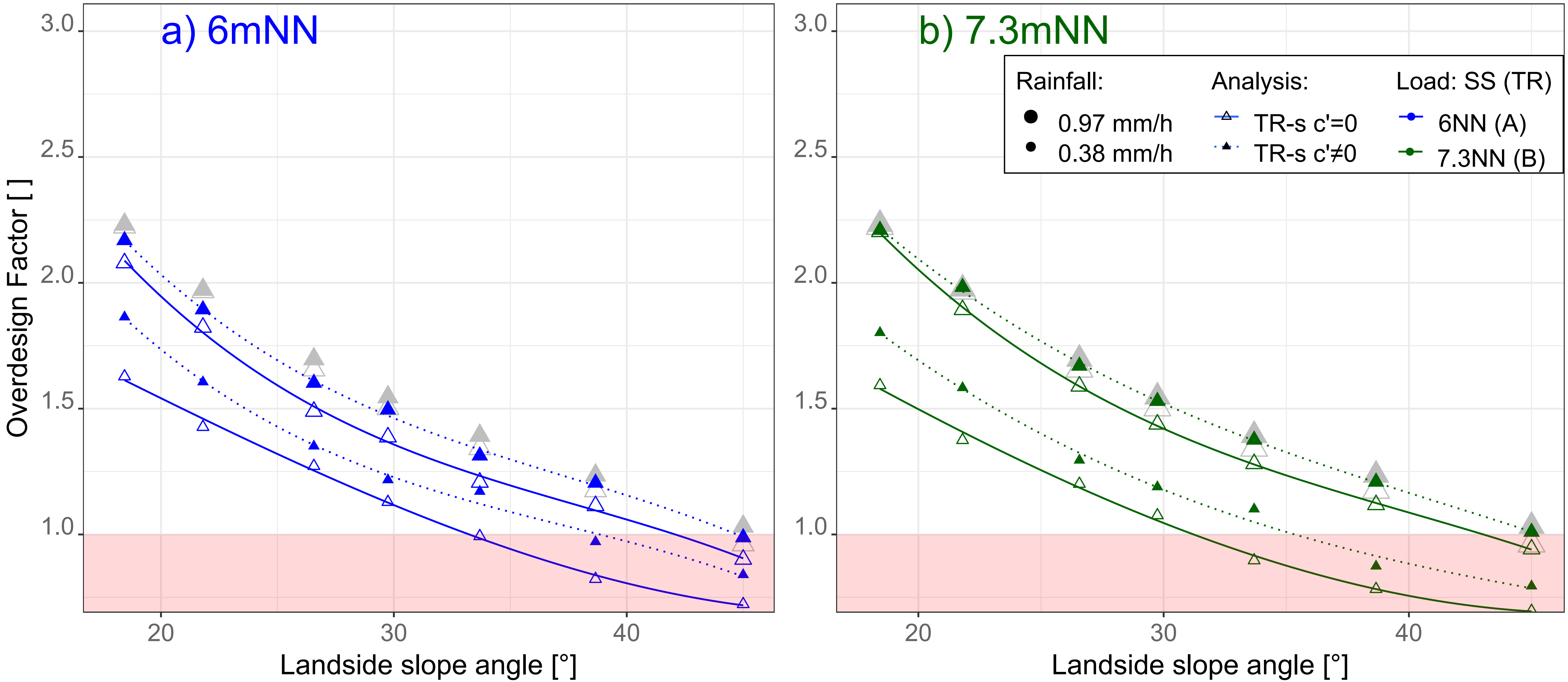

Retrofitted flood embankment

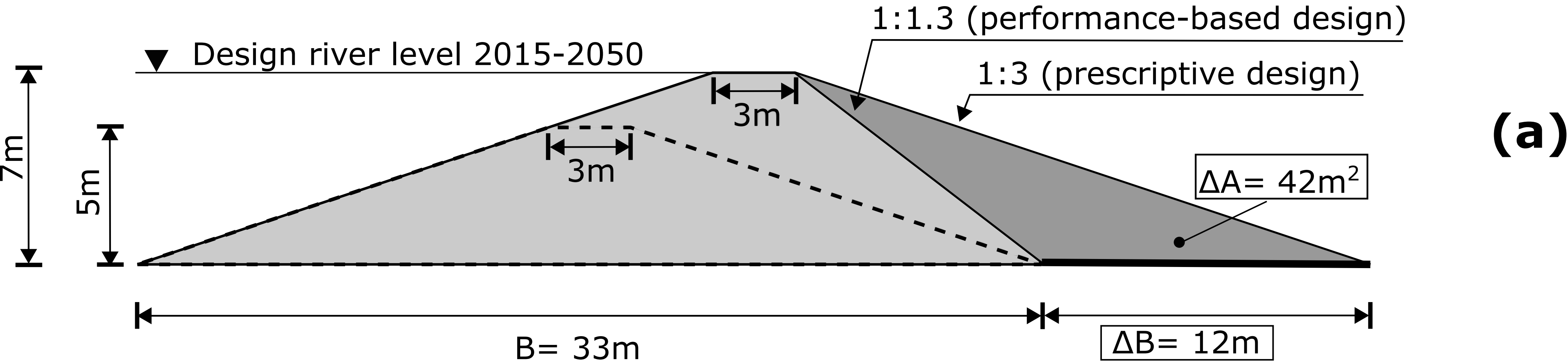

New flood embankment

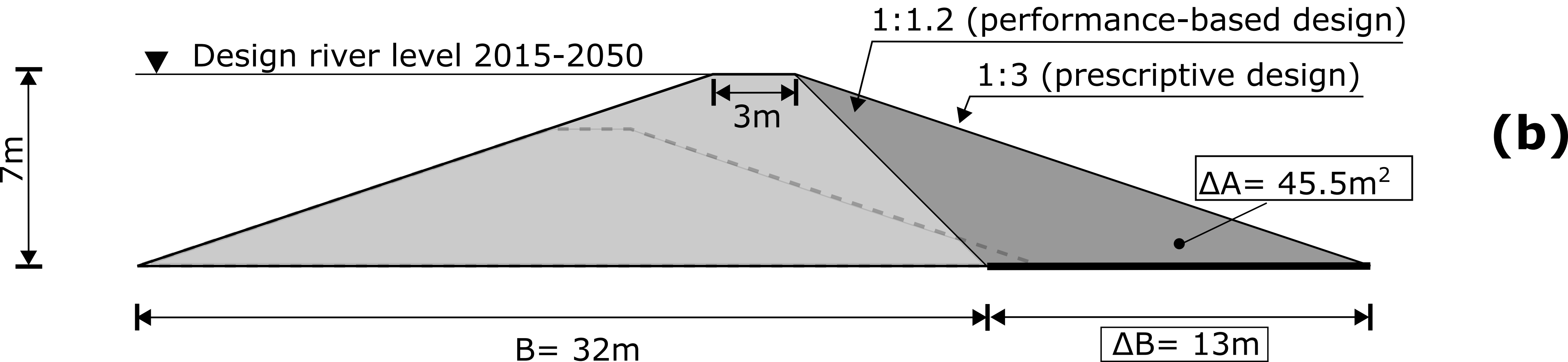

Fig15

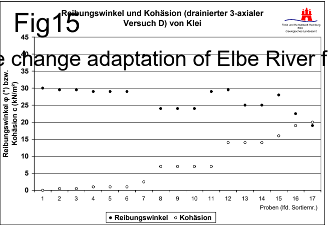

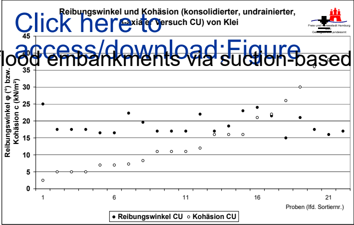

Click here to access/download;Figure;

e change adaptation of Elbe River flood embankments via suction-based

Fig16

Click here to access/download;Figure

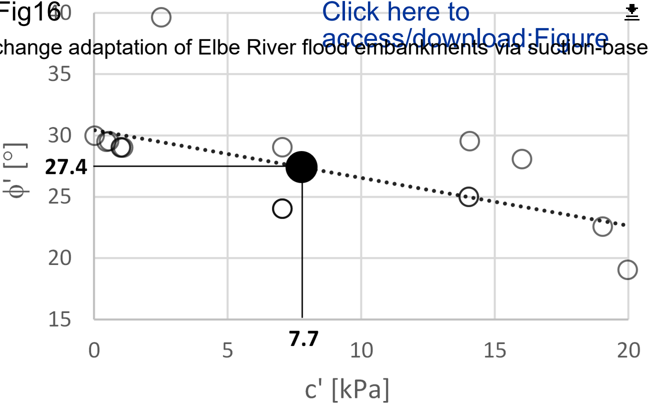

Fig17

e change adaptation of Elbe River flood embankments via suction-based

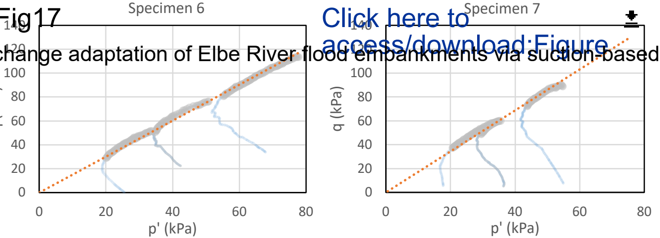

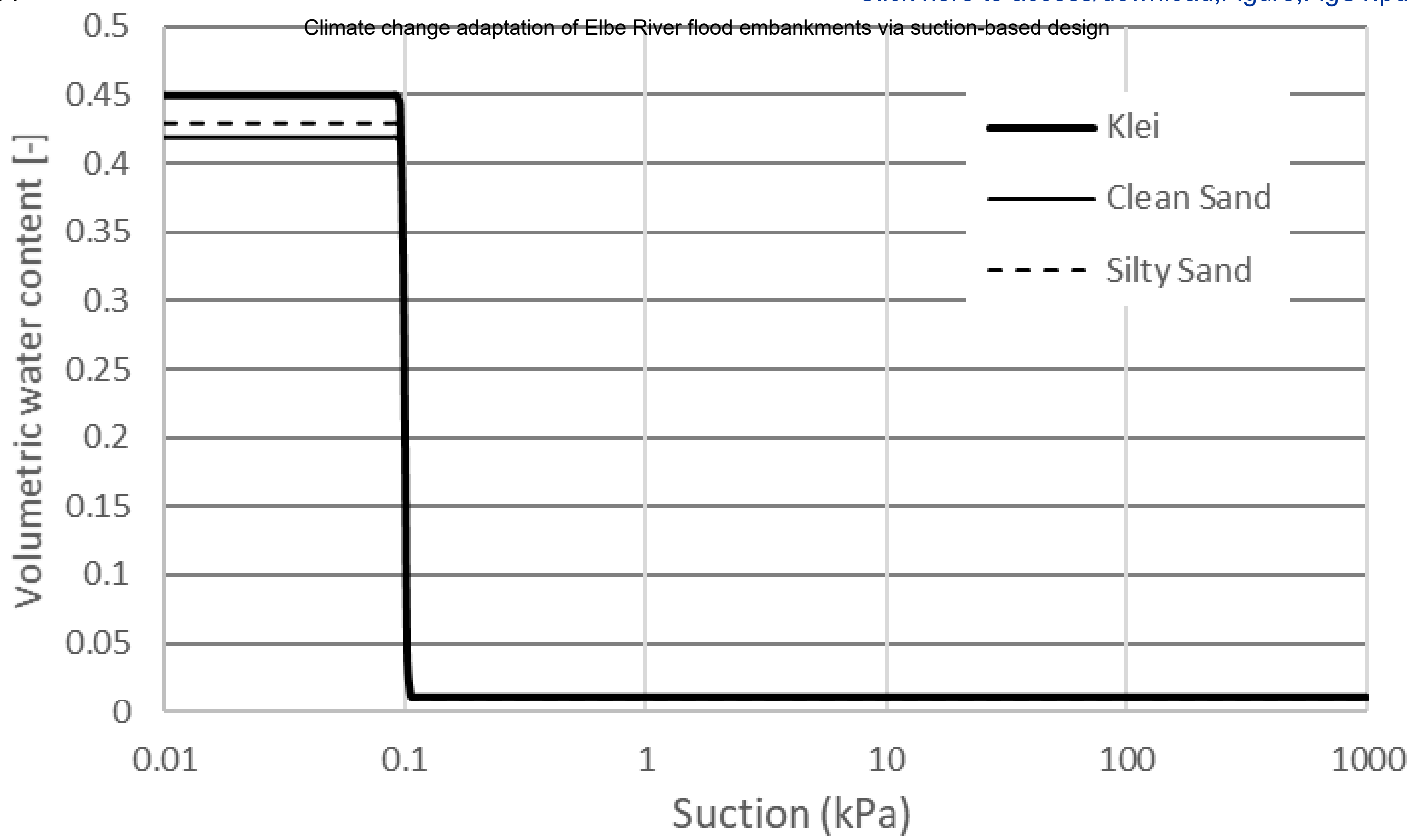

Climate change adaptation of Elbe River flood embankments via suction-based design
Volumetric water content [-]
0.5
0.45
0.4
0.35
0.3
0.25
0.2
0.15
0.1
0.05
0
0.01
0.1
1
10
100
1000
Suction (kPa)
Klei
Clean Sand
Silty Sand

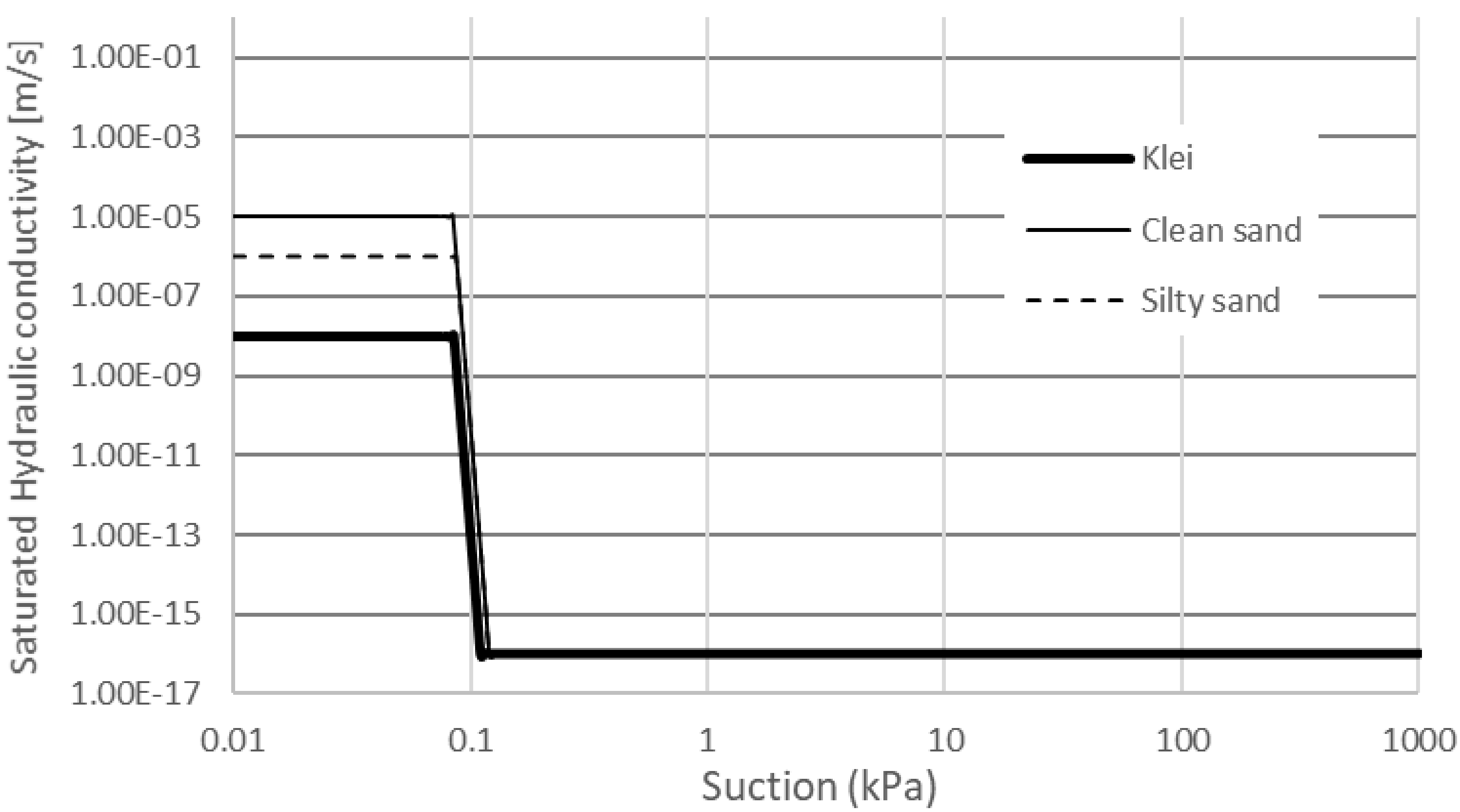

Saturated Hydraulic conductivity [m/s]
1.00E-01
1.00E-03
1.00E-05
1.00E-07
1.00E-09
1.00E-11
1.00E-13
1.00E-15
1.00E-17
0.01
0.1
1
10
100
1000
Suction (kPa)
Klei
Clean sand
Silty sand

FigS2

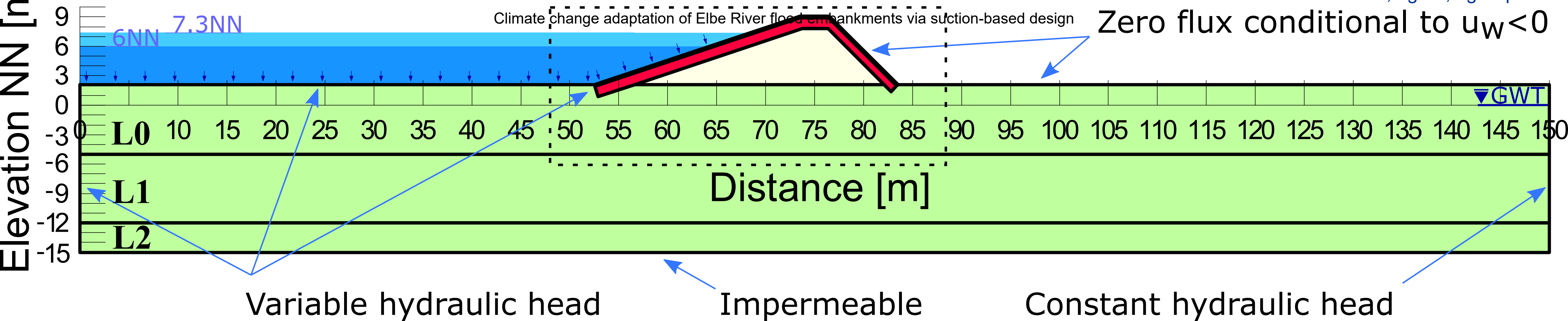

Climate change adaptation of Elbe River flood embankments via suction-based design
Elevation NN [m]
9
6
3
0
-3
-6
-9
-12
-15
7.3NN
6NN
Zero flux conditional to u_w<0
GWT
L0
L1
L2
0 10 15 20 25 30 35 40 45 50 55 60 65 70 75 80 85 90 95 100 105 110 115 120 125 130 135 140 145 150
Distance [m]
Variable hydraulic head
Impermeable
Constant hydraulic head

figS3

Climate change adaptation of Elbe River flood embankments via suction-based design

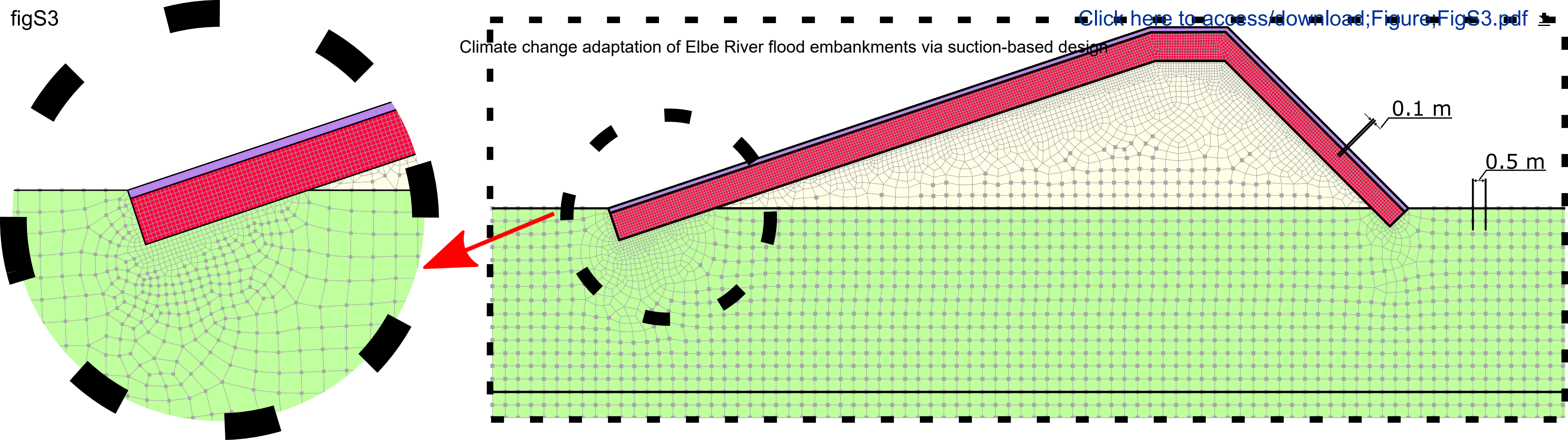

FigS4

e change adaptation of Elbe River flood embankments via suction-based

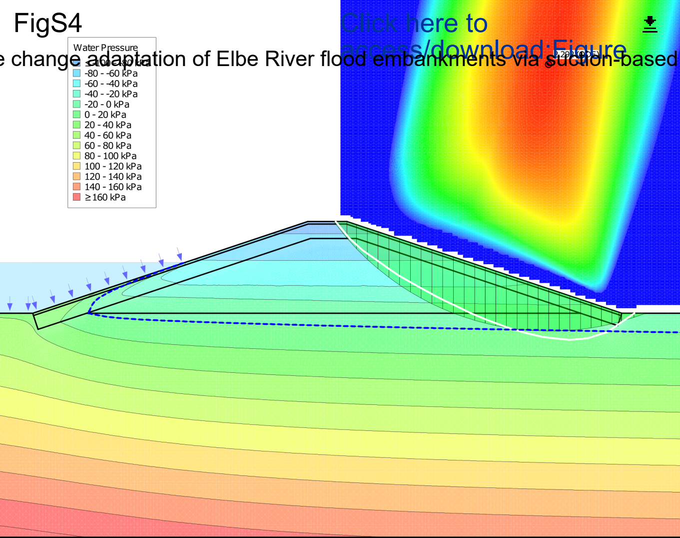

Figure 1. Geological cross section of the Hamburg Elbe harbour. (top) Uppermost layers consisting of Holocene klei & peat (pink) and Holocene silty sand (orange). (bottom) Representative schematic borehole logs. Original map taken from https://www.hamburg.de/bohrdaten-geologie

Figure 2 a) A-chain tide and b) B-peak tide used in the transient analysis, after Technische Rahmenbedingungen (TR HWS-Bau) by HPA (2008),

Figure 3. Geometry of the flood embankment (with the landside slope varied from 1:3 up to 1:1) and the layered foundation deposits analysed (L0, L1, and L2).

Figure 4. Representative grain size distributions of the materials forming the flood embankment and its foundation

Figure 5. Water retention functions adopted for the materials forming the flood embankment and its foundation.

Figure 6. Hydraulic boundary condition imposed on the water side for transient and steady-state analyses.

Figure 7. Stability analysis associated with river level at 6m NN for L0 scenario. (a) SS-Ns, Steady state analysis without suction effects, c'=0; (b) SS-Ns, Steady state analysis without suction effects, c' ≠ 0; (c) TR – Ns, Transient analysis with suction effects, c' = 0 (minimum ODF at 53.5h from the start of the storm surge); TR – Ns, Transient analysis with suction effects, c' ≠ 0 (minimum ODF at 53.5h from the start of the storm surge).

Figure 8. Effect of inclination of landside slope on Overdesign Factor for the homogenous silty sand foundation (scenario L0). (a) 6m NN – Pattern A (b) 7.3 m NN – Pattern B (SS-Ns= steady-state flow

with no suction effects; TR-s= steady-state flow with suction effects, open symbols → c'=0 and solid symbols → c'≠0)

Figure 9. Effect of inclination of landside slope on Overdesign Factor for the homogenous clayey foundation (scenario L1). (a) 6m NN – Pattern A (b) 7.3 m NN – Pattern B (SS-Ns= steady-state flow with no suction effects; TR-s= steady-state flow with suction effects, open symbols → c'=0 and solid symbols → c'≠0, grey shaded symbols refer to foundation scenario L0)

Figure 10. Effect of inclination of landside slope on Overdesign Factor for the confined silty sand foundation (scenario L1). (a) 6m NN – Pattern A (b) 7.3 m NN – Pattern B (SS-Ns= steady-state flow with no suction effects; TR-s= steady-state flow with suction effects, open symbols → c'=0 and solid symbols → c'≠0)

Figure 11. Effect of hydraulic conductivity of the Klei cover on the Overperformance Factor (foundation scenario L0). Saturated hydraulic conductivity increased from $k_{sat}=10^{-8}$ m/s to $k_{sat}=10^{-6}$ m/s. (SS-Ns= steady-state flow with no suction effect; TR-s= steady-state flow with suction effects, shaded grey symbols represent the case of $k_{sat}=10^{-8}$ m/s for comparison).

Figure 12. Cumulative rainfall versus aggregation time over 17-year observation period. Data measured at the Hamburg Weather Mast 1997–2014. Solid circle = max historical rainfall data, solid triangle = 95th percentile, solid square =99th and the absolute maximum taken from the PDFs for the total (left scale) and maximum/95 th percentile ratio versus aggregation time (right scale). (modified from Weder, 2017).

Figure 13. Effect of rainfall on the Overdesign Factor (foundation scenario L0). Rainfall 0.97mm/h for 100h duration and rainfall 0.38 mm/h for 30 d duration for the two design storm surges. Shaded grey triangles represent the foundation scenario L0 in the absence of rainfall for comparison.

Figure 14. Comparison between prescriptive design (dark grey) and performance-based design (light grey). (a) flood embankment retrofit with no footprint increase. (b) new flood embankment with 1:1,2 landside slope.

Figure 15. Shear strength data in terms of friction angle ϕ' and effective cohesion c' provided by the Hamburg Geological Survey. (a) CD triaxial test data from Klei samples (http://ingdata.hamburg.de/pdf/KLabf3axKohaeReibD_s.pdf) (b) CD triaxial test data from Klei samples (http://ingdata.hamburg.de/pdf/KLabf3axKohaeReibCU_s.pdf)

*Fi*gure 16. Friction angle f' versus effective cohesion c' derived from CD triaxial test data and average value for friction angle f' and effective cohesion c'.

Figure 17. Re-interpreted triaxial Consolidate-Undrained tests of specimen 6 (http://ingdata.hamburg.de/pdf/tvc-DBrue-B83-1,90-22,33-7,29.pdf) and 7(http://ingdata.hamburg.de/pdf/tvc-CND-B3-2,50-19,57-8,28.pdf) in figure 19b database (isotropic stress p' versus deviator stress q).

Figure S1. Step functions were adopted for the water retention and hydraulic conductivity functions to simulate dry/saturated conditions

Figure S2. Hydraulic boundary conditions including highest water river level considered for both steady-state and transient

Figure S3. Zoom from Figure S2, Unstructured mesh of quadrilateral and triangular elements. Mesh density in regions where higher gradients develop was optimised by reducing the element size until no significant change in simulated pore-water pressure was observed (~ 0.5 kPa). Elements with size equal to 0.1m were adopted for the embankment cover and elements with size equal to 0.5m were used for the embankment core and foundation layers

Figure S4. Stability analysis using the modified Bishop method (non-circular failure surface in white). The contour plot shows the Factor of Safety associated with the centre of the initially circular failure surface (before refinement) to check that the centre of the circular failure surface associated with the minimum Factor of Safety falls well within the grid inputted to search the critical failure surface.